typeset using JPSJ.sty <ver.0.7f>

Dimensional Crossovers in the Doped Ladder System: Spin Gap, Superconductivity and Interladder Coherent Band Motion

Jun-ichiro Kishine* and Kenji Yonemitsu

Department of Theoretical Studies, Institute for Molecular Science, Okazaki 444-8585, Japan

(Received December 5, 1997)

Based on the perturbative renormalization group (PRG) approach, we have studied dimensional crossovers in Hubbard ladders coupled via weak interladder one-particle hopping, $t_\perp$. We found that the one-particle crossover is strongly suppressed through growth of the intraladder scattering processes which lead the isolated Hubbard ladder system toward the spin gap metal (SGM) phase. Consequently when $t_\perp$ sets in, there exists, for any finite intraladder Hubbard repulsion, $U > 0$, the region where the two-particle crossover dominates the one-particle crossover and consequently the d-wave superconducting transition, which is regarded as a bipolaron condensation, occurs. By solving the scaling equations for the interladder one-particle and two-particle hopping amplitudes, we give phase diagrams of the system with respect to U, $t_{\perp 0}$ (initial value of $t_\perp$) and the temperature, T. We compared the above dimensional crossovers with those in a weakly coupled chain system, clarifying the difference between them.

KEYWORDS: doped ladder, dimensional crossover, perturbative renormalization-group, spin gap metal, bipolaron condensation, d-wave superconductivity

§1. Introduction

Magnetic and electronic properties of ladder materials have attracted great interest. [1] Central to these issues are the effects of the unusual spin-liquid state with a spin excitation gap in the undoped parent system on the electronic conduction in the doped system. Last year Uehara *et al.* [2] discovered a superconductivity signal in the doped ladder system, $Sr_{14-x}Ca_xCu_{24}O_{41}$, under pressure. The compound consists of the alternating stacks of planes with the CuO_2 chains and with the Cu_2O_3 two-leg ladders. The nominal valence of Cu is

* E-mail:kishine@ims.ac.jp

+2.25, independent of x, so the system is inherently doped with 6 holes in the unit, which are mainly on the chains at $x = 0$. Increase of the low-energy spectral weight [3] with increasing x indicates that the hole carriers are progressively redistributed from chains to ladders with Ca substitution for Sr. This feature was also confirmed theoretically through the ionic and cluster model calculations. [4] The behavior of the dc resistivity of the compounds changes from semiconducting-like to metal-like with Ca substitution, [2,5] and superconductivity sets in for $Sr_{0.4}Ca_{13.6}Cu_{24}O_{41}$ below $T_c = 12$ K under a pressure of 3 GPa. [2]

The spin excitation gap at the ladder cite in $Sr_{14}Cu_{24}O_{41}$ has been observed through NMR shifts and rates, [6, 7] and neutron scattering experiments. [8] A remarkable feature is that the spin gap in the ladder survives upon Ca substitution, [9, 10] indicating the doped ladder compounds, $Sr_{14-x}Ca_xCu_{24}O_{41}$, are in the *spin gap metal phase* which reflects the one-dimensional character of the ladder. According to the electronic structure calculation of $Sr_{14-x}Ca_xCu_{24}O_{41}$ under ambient pressure within the local-density approximation, [11] the interladder hoppings are 5-20 % of the intraladder ones, indicating a pseudo-one-dimensional character of the system.

The superconducting transition under pressure suggests that interladder one-particle hopping enhanced by applied pressure plays an important role. Recent experiments of the resistivity along the ladders, ρ_c, of the single crystal $Sr_{2.5}Ca_{11.5}Cu_{24}O_{41}$ by Akimitsu *et al.* [12] shows that the superconductivity sets in below 10 K under 3.5 GPa $\sim$ 8 GPa with the temperature dependence of ρ_c changing gradually from T-linear to T^2. The ratio of the normal state resistivity, ρ_c/ρ_a (ρ_a is resistivity perpendicular to the ladder direction in the ladder plane) also indicates a dimensional crossover from 1D to 2D with increasing applied pressure. [12]

The low-energy asymptotics of the isolated ladder system has been extensively studied mainly based on the renormalization-group approach, with and without the aid of the bosonization technique, to the two-leg Hubbard ladder [13,14,15,16,17,18,19] and the two-leg t-J ladder. [20, 21, 22, 23] In the isolated Hubbard ladder, the most relevant phase is characterized by a strong coupling fixed point and is denoted by "phase I" by Fabrizio [13] and "C1S0 phase" by Balents and Fisher. [16] In this phase, only the total charge mode remains gapless and consequently the d-wave superconducting correlation becomes the most dominant one [13, 15, 16, 17] and the $4k_F$-CDW correlation becomes sub-dominant one [15, 16, 17] at least when the intraladder correlation is weak. From now on, we call this strong coupling phase a "spin gap metal (SGM) phase". Within the bosonization scheme, exponents of the d-wave superconducting and the $4k_F$CDW correlations, K_S and K_C, satisfy the *duality relation*, $K_S \cdot K_C = 1$, suggesting the low-energy dynamics in the SGM phase is described with "*bipolarons*", each of which lies along the rung of the ladder. [21, 24] The enhancement of the d-wave superconducting channel has also been found by numerical studies on the two-leg Hubbard ladder through the density matrix renormalization group (DMRG) analysis, [25] the exact diagonalization study, [26] and the Monte-Carlo simulation. [27] The exact diagonalization study on the two-leg t-J ladder also gave evidences of a gapless total charge mode [28] and a d-wave RVB state [24, 29] in the doped system.

So far effects of the weak interladder hopping have been studied through mean field approximations [30,31] and power counting arguments. [32] Recently the present authors discussed effects of the interladder one-particle hopping, $t_\perp$, on the low-energy asymptotics of the weakly coupled Hubbard ladder system, based on the perturbative renormalization-group (PRG) approach and discussed dimensional crossovers in the system. [33]

Although the dimensional crossover problem in the coupled ladder system is rather new aspect, the similar problem in the coupled chain system has a history of about twenty years. [34,35,36] Effects of strong intrachain quantum fluctuations on the competition between one-particle and two-particle crossovers were first addressed by Brazovskii and Yakovenko. [37] It was pointed out by Suzumura, [38] based on the bosonization technique, that the two-particle crossover dominates the one-particle crossover only in the presence of large intrachain correlation. Recently the competition was again discussed in terms of the stiffness of the Tomonaga-Luttinger liquid. [39]

Bourbonnais and Caron, on the other hand, first discussed the problem based on the PRG approach, [40, 41, 42] where the intrachain interaction and interchain one-particle hopping are treated as perturbations to one-dimensional free fermion gas. In their formulation, the two-particle processes are generated by the interchain one-particle hopping *in the course of renormalization.* Based on their formulation, the dimensional crossovers in the weakly coupled chains were discussed in terms of the anomalous dimension of the Tomonaga-Luttinger liquid. [43]

In the present paper we extend discussions on the results we shortly presented in our previous paper. [33] Based on the PRG approach, we treated the *intraladder* interaction and the *interladder* one-particle hopping as perturbations to the free fermion gas on the ladder and obtained the phase diagram of the system. In this extended version, a full account of application of the PRG scheme to the dimensional crossover problem in the weakly coupled ladder system is given. Furthermore, we re-examine the dimensional crossovers in the weakly coupled chain system, clarifying the difference between the coupled ladders and chains. We show that the main difference comes from the different behaviors of the scaling flows of respective coupling strengths, i.e, the different universality classes of the corresponding isolated systems.

The outline of the present paper is as follows. In §2, we give a qualitative description of the notion of the one-particle and two-particle crossovers in the weakly coupled ladder system. In §3, we give a full account of formulation; the action, the scaling equations for the intraladder processes, the interladder one-particle process and the interladder two-particle process. In §4, based on the solutions of the scaling equations, we give phase diagrams of the system. In §5, we re-examine the dimensional crossover problem in the weakly coupled chains. In the final section, we give concluding remarks. Some technical details are left to Appendices.

§2. Dimensional Crossovers: One-Particle vs. Two-Particle Crossovers

The central problem here is how the weak interladder one-particle hopping, $t_\perp$, affects the low-energy asymptotics of the system. We switch on the intraladder interaction and the interladder one-particle hopping, $t_\perp$, as perturbations to the system specified by the intraladder longitudinal (transverse) hopping, $t(t')$ (see Fig. 1). [44] Then two kinds of interladder processes, a one-particle process and a two-particle process, occur. We illustrate these processes in Fig. 2. The one-particle and two-particle processes correspond to the interladder hopping of the single-particle excitation and that of the two-particle (particle-particle or particle-hole pair) excitation, respectively. As the temperature scale decreases, dimensional crossovers are induced by a one-particle process *or* a two-particle process. [37, 38, 39, 42] If the former dominates the latter, an interladder coherent band motion occurs. Then the character of the ladder in one-dimension is completely lost. On the other hand, if the latter dominates the former, interladder coherent propagation of a pair of composite particles

occurs and the system transits to a long-range-ordered phase in the corresponding channel. In Fig. 2, we show the two-particle hopping in the d-wave superconducting channel, which corresponds to the interladder Josephson tunneling of bipolarons. We will see this is the most dominant two-particle process.

The isolated doped ladder system has a spin excitation gap, which corresponds to the binding energy of the bipolaron. Thus the amplitude of the interladder tunneling of a bipolaron is roughly estimated as $t_\perp^2/\Delta_\sigma$, where Δ_σ is the characteristic energy scale of the spin gap. On the other hand, the amplitude of the one-particle hopping is $t_\perp$. Consequently, the competition is determined by the ratio, $t_\perp/\Delta_\sigma$, which is strongly affected by one-dimensional quantum fluctuations in the system.

§3. Scaling Equations for Interladder One-Particle and Two-Particle Hopping Amplitudes

To study the competition between the one-particle and two-particle crossovers, we set up scaling equations for the interladder one-particle and two-particle hopping amplitudes.

3.1 Action

We start with the path integral representation of the partition function of the system, $Z = \int \mathcal{D}e^S$, where the action consists of four parts,

$$S = S_\parallel^{(1)} + S_\parallel^{(2)} + S_\perp^{(1)} + S_\perp^{(2)}, \tag{3.1}$$

with $S_\parallel^{(1)}$, $S_\parallel^{(2)}$, $S_\perp^{(1)}$ and $S_\perp^{(2)}$ being the actions for the intraladder one-particle hopping, intraladder two-particle scattering, interladder one-particle and interladder two-particle hoppings, respectively. $\mathcal{D}$ symbolizes the measure of the path integral over the fermionic Grassmann variables.

The intraladder one-particle process is diagonalized with respect to the bonding (B) and antibonding (A) bands. As shown in Fig. 3(a), we linearize the dispersion along the legs on the bonding and antibonding Fermi points, $\pm k_{Fm} (m = A, B)$. In Fig. 3, R and L denote the right-moving and left-moving branches, respectively. The actions for the intra- and interladder one-particle hopping processes are written as

$$S_\parallel^{(1)} = \sum_K \sum_{m=A,B} \sum_\sigma \left[\mathcal{G}_{Lm}^{-1}(K_\parallel) L_{m\sigma}^*(K) L_{m\sigma}(K) + \mathcal{G}_{Rm}^{-1}(K_\parallel) R_{m\sigma}^*(K) R_{m\sigma}(K) \right], \tag{3.2}$$

and

$$S_\perp^{(1)} = -\sum_K \sum_{m=A,B} \sum_\sigma \varepsilon_{\perp m}(k_\perp) \left[L_{m\sigma}^*(K) L_{m\sigma}(K) + R_{m\sigma}^*(K) R_{m\sigma}(K) \right], \tag{3.3}$$

where $R_{m\sigma}(K)$ and $L_{m\sigma}(K)$ are the Grassmann variables representing the right- and left-moving electrons on the band m. The dispersions in the interladder action are given by $\varepsilon_{\perp A}(k_\perp) = +t_\perp \cos k_\perp$ and $\varepsilon_{\perp B}(k_\perp) = -t_\perp \cos k_\perp$. We use the notation $K = (k_\parallel, k_\perp, \mathrm{i}\varepsilon_n)$ and $K_\parallel = (k_\parallel, \mathrm{i}\varepsilon_n)$ where $\varepsilon_n = (2n+1)\pi/\beta$ is a fermion thermal frequency. We denote the momenta along the leg and the rung by $k_\parallel$ and $k_\perp$, respectively. The intraladder Green functions are written as

$$\mathcal{G}_{\nu m}(K_\parallel) = [\mathrm{i}\varepsilon_n - \varepsilon_{\nu m}(k_\parallel)]^{-1}, \tag{3.4}$$

where the linearized dispersions are given by $\varepsilon_{Rm}(k_\parallel) = v_F(k_\parallel - k_{Fm})$ and $\varepsilon_{Lm}(k_\parallel) = v_F(-k_\parallel - k_{Fm})$. The Fermi momenta of the bonding and antibonding bands are given by $k_{FB} = k_F +$

t'/v_F and $k_{FA} = k_F - t'/v_F$, respectively. The Fermi velocities in principle depend on the band index as $v_{Fm} = 2t \sin k_{Fm}$, but we assume throughout this work that $v_{Fm} = v_F$ and drop the band index, since the difference in the Fermi velocities does not affect the asymptotic nature of the SGM phase at least for small t'/t. [13, 16] In all the four branches(LB, LA, RA, RB) of linearized bands, the energy variables, $\varepsilon_{\nu m}(\nu = R, L; m = A, B)$, run over the region, $-E/2 < \varepsilon_{\nu m} < E/2$, with E denoting the *bandwidth cutoff*.

The intraladder Hubbard repulsion generates scattering processes depicted in Fig. 3(b). The action for the intraladder two-particle scattering processes is written as

$$\begin{aligned} S_{\parallel}^{(2)} = & \frac{2\pi v_F}{\beta} \sum g_0^{\sigma_1\sigma_2\sigma_3\sigma_4} L^*_{m\sigma_1} R^*_{m\sigma_2} R_{m\sigma_3} L_{m\sigma_4} + \frac{2\pi v_F}{\beta} \sum g_f^{\sigma_1\sigma_2\sigma_3\sigma_4} L^*_{m\sigma_1} R^*_{\bar{m}\sigma_2} R_{\bar{m}\sigma_3} L_{m\sigma_4} \\ & + \frac{2\pi v_F}{\beta} \sum g_t^{\sigma_1\sigma_2\sigma_3\sigma_4} L^*_{m\sigma_1} R^*_{m\sigma_2} R_{\bar{m}\sigma_3} L_{\bar{m}\sigma_4}, \end{aligned} \tag{3.5}$$

where the summations are taken over band indices, spins, intraladder momenta and frequencies as

$$\begin{aligned} & \sum L^*_{m_1\sigma_1} R^*_{m_2\sigma_2} R_{m_3\sigma_3} L_{m_4\sigma_4} \\ = & \sum_{K_1,\cdots,K_4} \sum_{m_1,\cdots,m_4} \sum_{\sigma_1,\cdots,\sigma_4} \delta(K_1 + K_2 - K_3 - K_4) L^*_{m_1\sigma_1}(K_1) R^*_{m_2\sigma_2}(K_2) R_{m_3\sigma_3}(K_3) L_{m_4\sigma_4}(K_4) \end{aligned}$$

with m and $\bar{m}$ being different band indices. The dimensionless intraladder scattering strengths are given by

$$g_\mu^{\sigma_1\sigma_2\sigma_3\sigma_4} = g_\mu^{(1)} \delta_{\sigma_1\sigma_3} \delta_{\sigma_2\sigma_4} - g_\mu^{(2)} \delta_{\sigma_1\sigma_4} \delta_{\sigma_2\sigma_3}, \tag{3.6}$$

where dimensionless quantities $g_\mu^{(1)}$ and $g_\mu^{(2)}$ denote backward and forward scattering strengths, respectively, with the flavor indices, [13] $\mu = 0, f, t$. The usual scattering strengths with dimension of the interaction energy are $2\pi v_F g_\mu^{(i)}$. We neglect the interband backward scattering terms like $\sum g_b^{\sigma_1\sigma_2\sigma_3\sigma_4} L^*_{B\sigma_1} R^*_{A\sigma_2} R_{B\sigma_3} L_{A\sigma_4}$ on the ground that these processes do not seriously modify the asymptotic nature of the C1S0 phase for finite t' [13, 16]. Since we neglect both of the band index dependence of the Fermi velocities and the interband backward processes, the intraladder transverse hopping, t', never appears explicitly in the present work.

The action for the interladder two-particle hopping processes are decomposed into CDWμ, SDWμ, SSμ (singlet superconducting) and TSμ (triplet superconducting) channels ($\mu = 0, f, t$ specify the corresponding flavor indices) as

$$\begin{aligned} S_{\perp}^{(2)} = & -\frac{\pi v_F}{2} \sum_{\mathrm{DW=CDW,SDW}} \sum \left[V_0^{\mathrm{DW}} \mathcal{O}_{\mathrm{DW}}^{mm*} \mathcal{O}_{\mathrm{DW}}^{mm} + V_t^{\mathrm{DW}} \mathcal{O}_{\mathrm{DW}}^{m\bar{m}*} \mathcal{O}_{\mathrm{DW}}^{\bar{m}m} + V_f^{\mathrm{DW}} \mathcal{O}_{\mathrm{DW}}^{m\bar{m}*} \mathcal{O}_{\mathrm{DW}}^{m\bar{m}} \right] \\ & - \frac{\pi v_F}{2} \sum_{\mathrm{S=SS,TS}} \sum \left[V_0^{\mathrm{S}} \mathcal{O}_{\mathrm{S}}^{mm*} \mathcal{O}_{\mathrm{S}}^{mm} + V_t^{\mathrm{S}} \mathcal{O}_{\mathrm{S}}^{mm*} \mathcal{O}_{\mathrm{S}}^{\bar{m}\bar{m}} + V_f^{\mathrm{S}} \mathcal{O}_{\mathrm{S}}^{\bar{m}m*} \mathcal{O}_{\mathrm{S}}^{\bar{m}m} \right], \end{aligned} \tag{3.7}$$

where V_μ^M denotes the interladder pair tunneling amplitude for channel $M\mu$. m and $\bar{m}$ denote different band indices. The summations are taken over band indices, intra- and inter-ladder momenta and boson thermal frequencies, $Q = (q_\parallel, q_\perp, \mathrm{i}\omega_l)$, with $\omega_l = 2l\pi/\beta$,

$$\sum V_\mu^M \mathcal{O}_M^{m_1 m_2 *} \mathcal{O}_M^{m_3 m_4} = \sum_Q \sum_{m_1,\cdots,m_4} V_\mu^M \mathcal{O}_M^{m_1 m_2 *}(Q) \mathcal{O}_M^{m_3 m_4}(Q).$$

The corresponding composite field variables are defined by

$$\begin{aligned}
\mathcal{O}^{mm'}_{\rm CDW}(Q) &= \beta^{-1/2}\sum R^*_{m\sigma}(K+Q)L_{m'\sigma}(K),\\
\vec{\mathcal{O}}^{mm'}_{\rm SDW}(Q) &= \beta^{-1/2}\sum R^*_{m\sigma}(K+Q)\vec{\sigma}_{\sigma\sigma'}L_{m'\sigma'}(K),\\
\mathcal{O}^{mm'}_{\rm SS}(Q) &= \beta^{-1/2}\sum \sigma R_{m\sigma}(-K+Q)L_{m'\bar{\sigma}}(K),\\
\vec{\mathcal{O}}^{mm'}_{\rm TS}(Q) &= \beta^{-1/2}\sum \sigma R_{m\sigma}(-K+Q)\vec{\sigma}_{\sigma\sigma'}L_{m'\bar{\sigma}'}(K),
\end{aligned} \tag{3.8}$$

where $\vec{\sigma}$ are Pauli matrices, $\bar{\sigma}=-\sigma$, and the summations are taken over spins and K.

3.2 Scaling of the intraladder two-particle scattering processes

The idea of scaling is to eliminate the short-wavelength degrees of freedom to relate effective actions at successive energy scales. Based on the bandwidth cutoff regularization scheme, we parametrize the cutoff as $E(l)=E_0e^{-l}$ with the scaling parameter, l, and study how the action is renormalized as l goes from zero to infinity. Details on the derivation of the scaling equations are left to the Appendices.

Scaling equations for the intraladder scattering vertices, $g^{(i)}_\mu$, are generally written as [34]

$$\frac{d\ln g^{(i)}_\mu(l)}{dl} = z^{(i)}_{\|\mu}(l) - 2z_\|(l). \tag{3.9}$$

Within the 3rd order PRG scheme, the first term on the r.h.s, $z^{(i)}_{\|\mu}(l)$, comes from the vertex correction diagrams represented in Figs. 4(a) and 4(b) for $i=1$ and 2, respectively. The field rescaling procedure (see Appendix A) requires the second term, $2z_\|$, to be

$$\begin{aligned}
z_\|(l) = {}& g_0^{(1)}(l)^2 + g_0^{(2)}(l)^2 + g_f^{(1)}(l)^2 + g_f^{(2)}(l)^2 + g_t^{(1)}(l)^2 + g_t^{(2)}(l)^2\\
& - g_0^{(1)}(l)g_0^{(2)}(l) - g_f^{(1)}(l)g_f^{(2)}(l) - g_t^{(1)}(l)g_t^{(2)}(l),
\end{aligned} \tag{3.10}$$

which comes from the intraladder self-energy diagrams represented in Fig. 4(c). We give a full detail on the derivation of $z_\|$ in Appendix B. The full expressions for the scaling equations, (3.9), are given by

$$\begin{aligned}
\frac{d}{dl}g_0^{(1)}(l) = {}& -2({g_0^{(1)}}^2 + g_t^{(1)}g_t^{(2)}) + 2(g_f^{(1)}{g_t^{(2)}}^2 - g_f^{(1)}g_t^{(1)}g_t^{(2)})\\
& -2g_0^{(1)}({g_0^{(1)}}^2 + {g_f^{(1)}}^2 + {g_t^{(1)}}^2 + {g_t^{(2)}}^2 - g_t^{(1)}g_t^{(2)}),
\end{aligned} \tag{3.11}$$

$$\begin{aligned}
\frac{d}{dl}g_0^{(2)}(l) = {}& -({g_0^{(1)}}^2 + {g_t^{(1)}}^2 + {g_t^{(2)}}^2) + 2(g_f^{(2)}{g_t^{(2)}}^2 - g_t^{(1)}g_t^{(2)}g_f^{(2)})\\
& +2{g_t^{(1)}}^2g_f^{(2)} - {g_0^{(1)}}^3 - {g_f^{(1)}}^2g_0^{(1)} - {g_t^{(1)}}^2g_f^{(1)} - 2g_0^{(2)}({g_t^{(1)}}^2 + {g_t^{(2)}}^2 - g_t^{(1)}g_t^{(2)}),
\end{aligned} \tag{3.12}$$

$$\begin{aligned}
\frac{d}{dl}g_f^{(1)}(l) = {}& -2({g_f^{(1)}}^2 + {g_t^{(1)}}^2 - g_t^{(1)}g_t^{(2)})\\
& +2(g_0^{(1)}{g_t^{(2)}}^2 - g_0^{(1)}g_t^{(1)}g_t^{(2)}) - 2g_f^{(1)}({g_0^{(1)}}^2 + {g_f^{(1)}}^2 + {g_t^{(1)}}^2 + {g_t^{(2)}}^2 - g_t^{(1)}g_t^{(2)}),
\end{aligned} \tag{3.13}$$

$$\begin{aligned}
\frac{d}{dl}g_f^{(2)}(l) = {}& -({g_f^{(1)}}^2 - {g_t^{(2)}}^2) + 2(g_0^{(2)}{g_t^{(2)}}^2 - g_t^{(1)}g_t^{(2)}g_0^{(2)})\\
& +2{g_t^{(1)}}^2g_0^{(2)} - {g_t^{(1)}}^2g_0^{(1)} - {g_0^{(1)}}^2g_f^{(1)} - {g_f^{(1)}}^3 - 2g_f^{(2)}({g_t^{(1)}}^2 + {g_t^{(2)}}^2 - g_t^{(1)}g_t^{(2)}),
\end{aligned} \tag{3.14}$$

$$\frac{d}{dl}g_t^{(1)}(l) = -2(2g_t^{(1)}g_f^{(1)} - g_t^{(1)}g_f^{(2)} - g_f^{(1)}g_t^{(2)} + g_0^{(1)}g_t^{(2)} + g_t^{(1)}g_0^{(2)})$$

$$+2(2g_t^{(1)}g_0^{(2)}g_f^{(2)} - g_0^{(1)}g_t^{(1)}g_f^{(2)} - g_f^{(1)}g_t^{(1)}g_0^{(2)}) \tag{3.15}$$
$$-2g_t^{(1)}({g_0^{(1)}}^2 + {g_0^{(2)}}^2 + {g_f^{(1)}}^2 + {g_f^{(2)}}^2 + {g_t^{(1)}}^2 + {g_t^{(2)}}^2 - g_0^{(1)}g_0^{(2)} - g_f^{(1)}g_f^{(2)} - g_t^{(1)}g_t^{(2)}),$$

$$\frac{d}{dl}g_t^{(2)}(l) = -2(g_0^{(1)}g_t^{(1)} + g_0^{(2)}g_t^{(2)} - g_f^{(2)}g_t^{(2)})$$
$$+2(2g_0^{(2)}g_f^{(2)}g_t^{(2)} - g_f^{(1)}g_0^{(2)}g_t^{(2)} - g_0^{(1)}g_f^{(2)}g_t^{(2)} + 2g_0^{(1)}g_f^{(1)}g_t^{(2)} - g_t^{(1)}g_f^{(1)}g_0^{(1)})$$
$$-2g_t^{(2)}({g_0^{(1)}}^2 + {g_0^{(2)}}^2 + {g_f^{(1)}}^2 + {g_f^{(2)}}^2 + {g_t^{(1)}}^2 + {g_t^{(2)}}^2 - g_0^{(1)}g_0^{(2)} - g_f^{(1)}g_f^{(2)} - g_t^{(1)}g_t^{(2)}), \tag{3.16}$$

where we omitted the argument l in the scattering strengths on the r.h.s. The same equations are obtained by setting $g_b^{(1)} = g_b^{(2)} = 0$ in Eq.(A5) of Ref.[13].

Starting with the Hubbard type initial condition,

$$g_\mu^{(i)}(0) = \tilde{U} \equiv U/4\pi v_F > 0, \tag{3.17}$$

the scaling equations lead to the *strong coupling* fixed point [13]

$$\begin{array}{ccc} g_0^{(1)*} = -1, & g_f^{(1)*} = 0, & g_t^{(1)*} = 1, \\ g_0^{(2)*} = -\frac{3-2\tilde{U}}{4}, & g_f^{(2)*} = \frac{1+2\tilde{U}}{4}, & g_t^{(2)*} = 1. \end{array} \tag{3.18}$$

To obtain a physical description of the fixed point, it is useful to analyze the isolated Hubbard ladder system by means of the bosonization technique. [13, 14, 15, 16, 17, 18, 38, 20, 21, 22, 23] We introduce the phase fields, $\phi_\nu(x)$ and $\theta_\nu(x)$, where $\phi_\nu(x)$ and $\frac{1}{\pi}\partial_x\theta_\nu(x)$ are conjugate,

$$\left[\phi_\nu(x), \frac{1}{\pi}\partial_y\theta_\mu(y)\right] = \mathrm{i}\delta_{\mu\nu}\delta(x-y). \tag{3.19}$$

The mode-indices, $\mu, \nu = \rho A$, ρB, σA, σB, represent the charge- and spin-modes on the bands A or B, respectively. The charge- and spin-modes are combined into the total-mode (0-mode) and the relative-mode (π-mode) as

$$\phi_{\rho\pm} = (\phi_{\rho B} \pm \phi_{\rho A})/\sqrt{2}, \quad \phi_{\sigma\pm} = (\phi_{\sigma B} \pm \phi_{\sigma A})/\sqrt{2}, \tag{3.20}$$

where $+$ and $-$ denote the 0-mode and π-mode, respectively. Then the "non-interacting " part [including the $g_\mu^{(i)}$ processes ($\mu = 0, f$) for $i = 1$ with parallel spins and those for $i = 2$] of the Hamiltonian for the isolated Hubbard ladder system is written as [13, 15, 16]

$$\mathcal{H}_0 = \sum_{\nu=\rho\pm,\sigma\pm} \int \frac{dx}{2\pi} \left[u_\nu K_\nu \left(\partial_x\theta_\nu\right)^2 + \frac{u_\nu}{K_\nu}\left(\partial_x\phi_\nu\right)^2 \right]. \tag{3.21}$$

The velocity, u_ν, and the stiffness, K_ν, of each mode are given by

$$u_\nu = v_F\sqrt{1-g_\nu^2}, \quad K_\nu = \sqrt{\frac{1+g_\nu}{1-g_\nu}}, \tag{3.22}$$

where

$$g_{\rho\pm} = (g_0^{(1)} - 2g_0^{(2)}) \pm (g_f^{(1)} - 2g_f^{(2)}), \quad g_{\sigma\pm} = g_0^{(1)} \pm g_f^{(1)}. \tag{3.23}$$

The low-energy asymptotics of the isolated Hubbard ladder system is characterized by the strong coupling fixed point of three scattering strengths, $g_t^{(1)*} = g_t^{(2)*} = -g_0^{(1)*} = 1$, which correspond to

$$1/K_{\rho-} = K_{\sigma+} = K_{\sigma-} = 0. \tag{3.24}$$

The scale-invariance of $K_{\rho+} = \sqrt{(1-2\tilde{U})/(1+2\tilde{U})}$ means that the total-charge mode remains gapless. On the other hand, $1/K_{\rho-} = 0$ and $K_{\sigma+} = K_{\sigma-} = 0$ mean that the phases $\theta_{\rho-}$ and $\phi_{\sigma\pm}$ are respectively locked, suggesting the corresponding modes acquire a gap. [13, 15] Therefore, in this phase, only the total charge mode remains gapless and consequently the d-wave superconducting correlation becomes the most dominant one [13, 15, 16, 17] and the $4k_F$-CDW correlation becomes sub-dominant one [15, 16, 17] at least when the intraladder correlation is weak. The phase characterized by this fixed point is denoted by the "phase I" by Fabrizio [13] and the "C1S0 phase" by Balents and Fisher. [16] Throughout the present paper we call this phase a spin gap metal (SGM) phase. Exponents of the d-wave superconducting and the $4k_F$-CDW correlations, K_S and K_C, in the SGM phase satisfy the *duality relation*, $K_S \cdot K_C = 1$, suggesting the low-energy dynamics in the SGM phase is described with *bipolarons*, each of which lies along the rung of the ladder. [21, 24]

3.3 Scaling of the interladder one-particle hopping amplitude

The scaling of the interladder one-particle process is fully determined by the intraladder self-energy effects. The scaling equation, represented in Fig. 5, is written as

$$\frac{d\ln t_\perp(l)}{dl} = 1 - z_\parallel(l). \tag{3.25}$$

We solve the equation with the initial condition,

$$t_\perp(0)/E_0 = \tilde{t}_{\perp 0}. \tag{3.26}$$

The scaling equation, (3.25), and the fixed point, (3.18), lead to

$$\frac{d\ln t_\perp(l)}{dl} \stackrel{l\to\infty}{\longrightarrow} -\tilde{U}^2/2 - 7/8, \tag{3.27}$$

and consequently $t_\perp(l)$ *becomes always irrelevant at the final stage of the scaling procedure.* However, at an early stage of scaling, the r.h.s of eq.(3.25) remains positive since the intraladder couplings do not grow sufficiently as yet and consequently $t_\perp(l)$ grows. The r.h.s of (3.25) changes its sign from positive to negative in the course of renormalization and then $\tilde{t}_\perp(l)$ begins to decrease and is finally scaled to zero.

If, in the course of the scaling, $\tilde{t}_\perp(l) \equiv t_\perp(l)/E_0$ attains an order of unity around some crossover value of the scaling parameter, $l_{\rm cross}$, qualitatively specified by

$$\tilde{t}_\perp(l_{\rm cross}) = 1, \tag{3.28}$$

the weakly coupled ladder picture breaks down. Then, the notion of "relevance" or "irrelevance" of the interladder one-particle hopping loses its literal meaning, since the PRG treatment for $t_\perp$ becomes inapplicable for $l > l_{\rm cross}$. If $l_{\rm cross}$ precedes the scaling parameter specifying the two-particle crossover, the interladder one-particle hopping becomes *coherent* and the system is regarded as scaled to a "two-dimensional" system via the one-particle crossover. [40, 41, 42]

In Fig. 6(a) we illustrate the scaling flows of $\tilde{t}_\perp(l)$ with a fixed value of the intraladder repulsion, $\tilde{U} = 0.3$, and $\tilde{t}_{\perp 0} = 0.01, 0.02, 0.03, 0.04$. The peak positions are independent of $\tilde{t}_{\perp 0}$ and the peak heights are proportional to $\tilde{t}_{\perp 0}$. In Fig. 6(b) we illustrate the scaling flows of $\tilde{t}_\perp(l)$ with a fixed initial value of the interladder one-particle hopping $\tilde{t}_{\perp 0} = 0.01$ and $\tilde{U} = 0.1, 0.2, 0.3, 0.4, 0.5$. The peak positions and heights are sensitive to $\tilde{U}$. We see from Fig.6 that for small $\tilde{U}$, $\tilde{t}_\perp(l)$ reaches unity even for small $\tilde{t}_{\perp 0}$, while for larger $\tilde{U}$, $\tilde{t}_\perp(l)$ are strongly suppressed and very large $t_\perp$ is required for $\tilde{t}_\perp(l)$ to attain an order of unity. As the intraladder correlations become stronger, the one-particle process is more severely suppressed.

3.4 Scaling of the interladder two-particle hopping amplitudes

The scaling equation for the interladder two-particle hopping amplitudes, V_μ^M, are generally written as

$$\frac{dV_\mu^M(l)}{dl} = f_\mu^M(l) + z_{\perp\mu}^M(l) V_\mu^M(l), \tag{3.29}$$

where f_μ^M denote the generators of V_μ^M for channels $M\mu$ (M = CDW, SDW, SS, TS and $\mu = 0$, f, t). Note that $z_{\perp\mu}^M$ has $[V_\mu^M]^n$ contributions with $n = 0$ and $n = 1$. In Figs.7(a) and 7(b), we show the diagrammatic representation of f_μ^M for M = CDW/SDW and SS/TS, respectively. In Appendix C, we give the details on the derivation of f_μ^M.

The leading-order scaling equations for V_μ^M are diagrammatically given in Figs. 8(a) and 8(b), for M =CDW/SDW and SS/TS, respectively. Full expressions for the scaling equations, (3.29), are written as

$$\frac{dV_0^{\rm DW}(l)}{dl} = \frac{1}{4}\left[\tilde{t}_\perp(l) g_0^{\rm DW}(l)\right]^2 \cos q_\perp + g_0^{\rm DW}(l) V_0^{\rm DW}(l) - \frac{1}{2} V_0^{\rm DW}(l)^2, \tag{3.30}$$

$$\begin{aligned}\frac{dV_f^{\rm DW}(l)}{dl} = & -\frac{1}{4}\tilde{t}_\perp(l)^2 \left[g_t^{\rm DW}(l)^2 + g_f^{\rm DW}(l)^2\right] \cos q_\perp \\ & + g_t^{\rm DW}(l) V_t^{\rm DW}(l) + g_f^{\rm DW}(l) V_f^{\rm DW}(l) - \frac{1}{2}\left[V_t^{\rm DW}(l)^2 + V_f^{\rm DW}(l)^2\right],\end{aligned} \tag{3.31}$$

$$\begin{aligned}\frac{dV_t^{\rm DW}(l)}{dl} = & -\frac{1}{2}\tilde{t}_\perp(l) g_t^{\rm DW}(l) g_f^{\rm DW}(l) \cos q_\perp \\ & + g_t^{\rm DW}(l) V_f^{\rm DW}(l) + g_f^{\rm DW}(l) V_t^{\rm DW}(l) - V_t^{\rm DW}(l) V_f^{\rm DW}(l),\end{aligned} \tag{3.32}$$

$$\begin{aligned}\frac{dV_0^{\rm S}(l)}{dl} = & -\frac{1}{4}\tilde{t}_\perp(l)^2 \left[g_0^{\rm S}(l)^2 + g_t^{\rm S}(l)^2\right] \cos q_\perp + g_0^{\rm S}(l) V_0^{\rm S}(l) + g_t^{\rm S}(l) V_t^{\rm S}(l) \\ & - \frac{1}{2}\left[V_0^{\rm S}(l)^2 + V_t^{\rm S}(l)^2\right],\end{aligned} \tag{3.33}$$

$$\frac{dV_f^{\rm S}(l)}{dl} = \frac{1}{4}\tilde{t}_\perp(l)^2 g_f^{\rm S}(l)^2 \cos q_\perp + g_f^{\rm S}(l) V_f^{\rm S}(l) - \frac{1}{2} V_f^{\rm S}(l)^2, \tag{3.34}$$

$$\frac{dV_t^{\rm S}(l)}{dl} = -\frac{1}{2}\tilde{t}_\perp(l)^2 g_0^{\rm S}(l) g_t^{\rm S}(l) \cos q_\perp + g_0^{\rm S}(l) V_t^{\rm S}(l) + g_t^{\rm S} V_0^{\rm S}(l) - V_0^{\rm S}(l) V_t^{\rm S}(l), \tag{3.35}$$

with DW=CDW/SDW and S=SS/TS. Coupling strengths of the composite particles in these channels are given by

$$\begin{cases} g_\mu^{\rm CDW}(l) = g_\mu^{(2)}(l) - 2g_\mu^{(1)}(l), \quad g_\mu^{\rm SDW}(l) = g_\mu^{(2)}(l), \\ g_\mu^{\rm SS}(l) = -g_\mu^{(1)}(l) - g_\mu^{(2)}(l), \quad g_\mu^{\rm TS}(l) = g_\mu^{(1)}(l) - g_\mu^{(2)}(l). \end{cases} \tag{3.36}$$

We here introduce the composite fields of the s- and d-wave superconducting channels by [13, 15, 16, 17, 20, 21, 23]

$$\mathcal{O}_{\mathrm{SC}s} = \mathcal{O}_{\mathrm{SS}}^{BB} + \mathcal{O}_{\mathrm{SS}}^{AA}, \quad \mathcal{O}_{\mathrm{SC}d} = \mathcal{O}_{\mathrm{SS}}^{BB} - \mathcal{O}_{\mathrm{SS}}^{AA}. \tag{3.37}$$

Cooper pairs in the d-wave channel (=bipolaron on the rung) are formed on the adjacent legs on the same rung (see Fig. 2). The corresponding two-particle hopping amplitudes are constructed as

$$V^{\mathrm{SC}s}(l) = \frac{1}{2}\left[V_0^{\mathrm{SS}}(l) + V_t^{\mathrm{SS}}(l)\right], \quad V^{\mathrm{SC}d}(l) = \frac{1}{2}\left[V_0^{\mathrm{SS}}(l) - V_t^{\mathrm{SS}}(l)\right], \tag{3.38}$$

that satisfy the scaling equations

$$\frac{dV^{\mathrm{SC}s}}{dl} = -\left[\tilde{t}_\perp(l) g^{\mathrm{SC}s}(l)\right]^2 \cos q_\perp + 2 g_0^{\mathrm{SC}s}(l) V^{\mathrm{SS}s}(l) - \frac{1}{2} V^{\mathrm{SS}s}(l)^2, \tag{3.39}$$

$$\frac{dV^{\mathrm{SC}d}}{dl} = -\left[\tilde{t}_\perp(l) g^{\mathrm{SC}d}(l)\right]^2 \cos q_\perp + 2 g_0^{\mathrm{SC}d}(l) V^{\mathrm{SC}d}(l) - \frac{1}{2} V^{\mathrm{SC}d}(l)^2, \tag{3.40}$$

with the coupling strengths

$$g^{\mathrm{SC}s}(l) = \frac{1}{2}\left[g_0^{\mathrm{SS}}(l) + g_t^{\mathrm{SS}}(l)\right], \quad g^{\mathrm{SC}d}(l) = \frac{1}{2}\left[g_0^{\mathrm{SS}}(l) - g_t^{\mathrm{SS}}(l)\right], \tag{3.41}$$

which are scaled to the fixed point,

$$g^{\mathrm{SC}s*} = -(1 + 2\tilde{U})/8, \quad g^{\mathrm{SC}d*} = (15 - 2\tilde{U})/8. \tag{3.42}$$

We have solved simultaneously the scaling equations, (3.11) $\sim$ (3.16), (3.25), (3.30) $\sim$ (3.35), (3.39) and (3.40) with the initial conditions

$$g_\mu^{(i)}(0) = U/4\pi v_F \equiv \tilde{U}, \quad t_\perp(0)/E_0 = \tilde{t}_{\perp 0}, \quad V_\mu^M(0) = 0. \tag{3.43}$$

We put $q_\perp = 0$ and $q_\perp = \pi$ for the superconducting and density-wave channels, respectively. In Figs.9(a) $\sim$ (c), we show the scaling flows of the coupling strengths for the composite fields, (3.36), and $V_\mu^M(l)$ for $\tilde{U} = 0.2, 0.3, 0.4$ and $\tilde{t}_{\perp 0} = 0.01$, where the vertical broken line corresponds to the scaling parameter at which $V^{\mathrm{SC}d}$ diverges. We clearly see that the divergence of $V^{\mathrm{SC}d}$ always occurs at the highest energy scale. This situation is quite reasonable on physical grounds that the interladder pair tunneling stabilizes the most dominant intraladder correlation, i.e, the d-wave superconducting correlation. As is seen from Figs. 9(d) $\sim$ (f), the competition among the channels other than the SCd channel is rather subtle. Below we focus on the d-wave superconducting channel.

The first, second and the third terms on the r.h.s of eq.(3.40) play separate roles in the early, intermediate and final stages of the scaling of $V^{\mathrm{SC}d}$. At the early stage, the first term generates a finite magnitude of $V^{\mathrm{SC}d}$. At the intermediate stage, the second term induces an exponential growth of $V^{\mathrm{SC}d}$. At the final stage, the third term causes divergence of $V^{\mathrm{SC}d}$ at a critical scaling parameter l_c defined by

$$V^{\mathrm{SC}d}(l_c) = -\infty. \tag{3.44}$$

§4. Phase Diagram of Weakly Coupled Hubbard Ladders

Based on the scaling flows of $\tilde{t}_\perp(l)$ and $V^{\mathrm{SC}d}$, we show the competition between the one- and two-particle crossovers. The scaling flows of the intraladder system toward the SGM phase are best

visualized through the scaling flow of $K_{\sigma+}$, the stiffness of the total-spin mode. We here again note that $K_{\sigma+}=0$ corresponds to the fully developed spin gap at the low-energy limit. In Fig. 10, we illustrate the scaling flows of $K_{\sigma+}$, $\tilde{t}_\perp(l)$ and $V^{\mathrm{SC}d}$ with various initial conditions. We see from Fig. 10 that, for $(\tilde{U},\tilde{t}_{\perp 0})$ =(0.3,0.01), (0.3,0.02), (0.4,0.01) and (0.5,0.01), the two-particle crossover occurs at $l=l_c$. On the other hand, for $(\tilde{U},\tilde{t}_{\perp 0})$ =(0.3,0.03), (0.3,0.04), (0.1,0.01) and (0.2,0.01), $\tilde{t}_\perp(l)$ exceeds unity at l_{cross} before $V^{\mathrm{SC}d}$ diverges. Then the one-particle crossover occurs.

The scaling parameter is identified with the absolute temperature as $l=\ln\frac{E_0}{T}$. Thus we define the one-particle *crossover temperature*, T_{cross}, and the d-wave superconducting *transition temperature*, T_c, as

$$\begin{aligned} T_{\mathrm{cross}} &= E_0 e^{-l_{\mathrm{cross}}}, \\ T_c &= E_0 e^{-l_c}. \end{aligned} \tag{4.1}$$

We obtain phase diagrams of the system with respect to $(\tilde{U},\tilde{t}_{\perp 0})$ and the reduced temperature, $\tilde{T}=T/E_0$.

4.1 $t_{\perp 0}$-T phase diagram

First we show, in Fig. 11, the phase diagram spanned by $\tilde{t}_{\perp 0}$ and $\tilde{T}$ for $\tilde{U}=0.3$. Roughly speaking, we may regard increasing $\tilde{t}_{\perp 0}$ as applying the pressure, under which the bulk superconductivity was actually observed in a doped spin ladder, $Sr_{14-x}Ca_xCu_{24}O_{41}$. [2, 12] We found that there exists a crossover value of the interladder one-particle hopping, $\tilde{t}_{\perp c}\sim 0.025$.

For $0<\tilde{t}_{\perp 0}<\tilde{t}_{\perp c}$, the phase transition into the d-wave superconducting (SCd) phase occurs at a finite transition temperature, T_c, via the condensation of bipolarons driven by the two-particle crossover. In the temperature region, $T<T_c$, interladder coherent Josephson tunneling of the bipolarons occurs. Now we must use caution in identifying the finite temperature phase above T_c, where the system is in the *isolated ladder regime.* As the temperature scale decreases, the isolated ladder systems are *gradually* scaled to their low-energy asymptotics, the SGM phase, toward the zero temperature. The gradual change of darkness in the SGM phase in Fig.11 schematically illustrates this situation. The SGM phase is characterized by the strong coupling fixed point of intraladder scattering strengths, $g_t^{(1)}=g_t^{(2)}=-g_0^{(1)}=1$, or $1/K_{\rho-}=K_{\sigma+}=K_{\sigma-}=0$ (see (3.18) and (3.24)). We see from Fig.10 that the critical scaling parameter l_c is always in the region around which $K_{\sigma+}$ almost reaches its fixed point value. Thus we expect that the spin gap is well developed near T_c and the phase transition at T_c can be identified with the transition from the SGM phase to the SCd phase. Within the framework of the PRG approach, however, we cannot say for certain whether the spin gap survives in the SCd phase or not.

For $\tilde{t}_{\perp c}<\tilde{t}_{\perp 0}$, the system undergoes the crossover to the 2D phase via the one-particle crossover. The temperature scale of the one-particle crossover is not low enough to ensure a well-developed spin gap since the one-particle crossover takes place at an early stage of scaling, where the intraladder couplings are still far away from their strong coupling values, as can be seen from Fig.10. Thus it is disputable to assign the phase above T_{cross} to the SGM phase. In the temperature region, $T<T_{\mathrm{cross}}$ the transverse *coherent* band motion occurs. In section 4.4, we give brief comments on the physical nature of the 2D phase.

In this paper, we consider the case where t' is much larger than $t_{\perp 0}$ and is not so large as only one band to cut the Fermi surface (these conditions are actually satisfied in the real $Sr_{14-x}Ca_xCu_{24}O_{41}$ compounds [11]). Then, the (hypothetical) isolated ladder system is always scaled to the SGM phase. When t' decreases and becomes comparable to $t_{\perp 0}$, the system may be regarded as a coupled chain system, since, in such a case, the alternation of the transverse hopping would be

unimportant. As we shall discuss in §5, in the coupled chain system, the one-particle crossover converts the system to the 2D phase as far as $\tilde{U}$ is not extremely large. Then the SCd region would shrink with increasing t' to be connected with the case of comparable t' and $t_{\perp 0}$. However, our result (Fig. 11) would not be qualitatively changed.

4.2 U-T phase diagram

In Fig. 12, we show the phase diagram spanned by $\tilde{U}$ and $\tilde{T}$ for $\tilde{t}_{\perp 0} = 0.01$. We see that there exists a crossover value of the intraladder repulsion, $\tilde{U}_c \sim 0.22$. For $0 < \tilde{U} < \tilde{U}_c$, the system undergoes the crossover to the 2D phase via the one-particle crossover, while for $\tilde{U}_c < \tilde{U}$, the SGM phase transits to the SCd phase via the two-particle crossover.

4.3 Crossover values of the interladder one-particle hopping: $\tilde{t}_{\perp c}$

In Fig. 13, we show how the crossover value, $\tilde{t}_{\perp c}$, introduced in Fig. 11, depends on $\tilde{U}$. For $\tilde{t}_{\perp 0} > \tilde{t}_{\perp c}$, the system undergoes the crossover to the 2D phase, while for $\tilde{t}_{\perp 0} < \tilde{t}_{\perp c}$, the SGM phase transits to the SCd phase. $\tilde{t}_{\perp c}$ is always finite for $\tilde{U} > 0$ and becomes zero only for $\tilde{U} = 0$. Thus we see that *the crossover value, $\tilde{t}_{\perp c}$, always exists for $\tilde{U} > 0$*. The SCd phase vanishes only for $\tilde{U} = 0$, where the scaling equation, (3.25), gives $\tilde{T}_{\rm cross} = \tilde{t}_{\perp 0}$.

4.4 Remarks on the 2D phase

Here we give a few remarks on the 2D phase. In the 2D phase the physical properties of the system would strongly depend on the shape of the 2D Fermi surface which may be characterized by the misfit of the rungs in the neighboring ladders which actually exists in real $Sr_{14-x}Ca_xCu_{24}O_{41}$ compounds (see Fig. 14(a)). The band structure of the system is characterized by bonding (B) and antibonding (A) dispersions,

$$\varepsilon_{A,B}(\vec{k}) = -2t\cos k_{\parallel} \pm \sqrt{t'^2 + 4t''^2\cos^2\frac{k_{\perp}}{2} + 2t't''\cos\frac{k_{\perp}}{2}\cos k_{\parallel}}, \tag{4.2}$$

where the + and − signs are taken for A and B bands, respectively. It was pointed out by Yamaji [47] that in the two-dimensional two-band system, a superconducting transition is possible via the so-called Suhl-Kondo mechanism, [48, 49] where the interband exchange-like interaction is strongly enhanced by an *interband nesting*. Then the pairing interaction is caused by the processe expressed by the interband particle-hole ladder diagrams. Quite recently it was reported [50] that, by using a numerical fluctuation-exchange (FLEX) method, a superconducting transition actually becomes possible in a coupled Hubbard ladder system with the same configuration as that shown in Fig. 14(a), where the two-band structure of the system is taken into account.

To check how the interband polarization is enhanced by the interband nesting, we calculate the static interband polarization function written as

$$\chi_{AB}(q_{\parallel}, q_{\perp}) = \frac{1}{2}\sum_{\vec{k}} \frac{\tanh[\frac{\beta}{2}(\varepsilon_A(\vec{k}+\vec{q}/2)-\mu)] - \tanh[\frac{\beta}{2}(\varepsilon_B(\vec{k}-\vec{q}/2)-\mu)]}{\varepsilon_A(\vec{k}+\vec{q}/2) - \varepsilon_B(\vec{k}-\vec{q}/2)}, \tag{4.3}$$

In Fig. 14(b), we show $\chi_{AB}(q_{\parallel}, q_{\perp})$ on the 1st Brillouin zone along the line $\Gamma(0,0) \to {\rm X}(\pi, 0) \to {\rm M}(\pi,\pi) \to \Gamma$ for for $t = t'$ and $t''/t = 0, 0.2, 0.3$ with a chemical potential $\mu = 0$ and a temperature, $\beta^{-1} = T = 10^{-5}t$. We see that an increasing t'' decreases the degree of interband nesting and consequently the interband polarization function decreases. Then the exchange-like pairing interaction would also decrease. Thus, when a superconducting transition via Suhl-Kondo mechanism becomes possible in the 2D phase, the supercondicting transition temperature, T_c, should decrease with an increasing interladder coupling.

§5. Comparison with Dimensional Crossovers in Weakly Coupled Chains

In this section we compare the dimensional crossovers in the present system with those in the weakly coupled Hubbard chains. Although the PRG approach to the dimensional crossover problem for the weakly coupled chains has been extensively studied by Broubonnais and Caron, [42] it is instructive to re-examine their work, clarifying the difference in the nature of the dimensional crossovers in the two cases.

The action for the weakly coupled chain system consists of four parts,

$$S_{\rm chain} = S^{(1)}_{{\rm chain}\parallel} + S^{(2)}_{{\rm chain}\parallel} + S^{(1)}_{{\rm chain}\perp} + S^{(2)}_{{\rm chain}\perp}, \tag{5.1}$$

where $S^{(1)}_{{\rm chain}\parallel}$, $S^{(2)}_{{\rm chain}\parallel}$, $S^{(1)}_{{\rm chain}\perp}$ and $S^{(2)}_{{\rm chain}\perp}$ denote the actions for the intrachain one-particle hopping, intrachain two-particle scattering, interchain one-particle and interchain two-particle hoppings, respectively. As shown in Fig. 15(a), we linearize the dispersion along the chains on the two Fermi points, $\pm k_F$. The intrachain Hubbard repulsion generates scattering processes depicted in Fig. 15(b). The processes are specified by dimensionless quantities $g^{(1)}$ and $g^{(2)}$ denoting backward and forward scattering strengths, respectively. [34] The usual scattering strengths with dimension of the interaction energy are $\pi v_F g^{(i)}$.

The action for the interchain two-particle hopping processes are decomposed into CDW, SDW, SS(singlet superconducting) and TS(triplet superconducting) channels and is written, instead of (3.7), as

$$S^{(2)}_{{\rm chain}\perp} = -\frac{\pi v_F}{4} \sum_{\rm D=CDW,SDW} \sum_{Q} V^{\rm D} \mathcal{O}^*_{\rm D} \mathcal{O}_{\rm D} - \frac{\pi v_F}{4} \sum_{\rm S=SS,TS} \sum_{Q} V^{\rm S} \mathcal{O}^*_{\rm S} \mathcal{O}_{\rm S}, \tag{5.2}$$

where V^M denotes the amplitude of the interchain two-particle hopping for channel M. The corresponding composite field variables are defined by

$$\begin{aligned}
\mathcal{O}_{\rm CDW}(Q) &= \beta^{-1/2} \sum R^*_\sigma(K+Q) L_\sigma(K), \\
\vec{\mathcal{O}}_{\rm SDW}(Q) &= \beta^{-1/2} \sum R^*_\sigma(K+Q) \vec{\sigma}_{\sigma\sigma'} L_{\sigma'}(K), \\
\mathcal{O}_{\rm SS}(Q) &= \beta^{-1/2} \sum \sigma R_\sigma(-K+Q) L_{\bar\sigma}(K), \\
\vec{\mathcal{O}}_{\rm TS}(Q) &= \beta^{-1/2} \sum \sigma R_\sigma(-K+Q) \vec{\sigma}_{\sigma\sigma'} L_{\bar\sigma'}(K),
\end{aligned} \tag{5.3}$$

where $\vec{\sigma}$ are Pauli matrices, $\bar\sigma = -\sigma$, and the summations are taken over spins and K with $K = (k_\parallel, k_\perp, {\rm i}\varepsilon_n)$ for each $Q = (q_\parallel, q_\perp, {\rm i}\omega_l)$ with fermion and boson thermal frequencies, $\varepsilon_n = (2n+1)\pi/\beta$ and $\omega_l = 2l\pi/\beta$, respectively. We denote the momenta along and perpendicular to the chains by $k_\parallel$ and $k_\perp$, respectively.

The diagrams which give the scaling equations for the intrachain scattering processes are the same as in Fig. 4, but some of them are canceled out to give, instead of (3.11) $\sim$ (3.16), simple scaling equations [34]

$$\frac{dg^{(1)}(l)}{dl} = -g^{(1)}(l)^2 - \frac{1}{2} g^{(1)}(l)^3, \tag{5.4}$$

$$\frac{dg^{(2)}(l)}{dl} = -\frac{1}{2} g^{(1)}(l)^2 - \frac{1}{4} g^{(1)}(l)^3. \tag{5.5}$$

Starting with the Hubbard type initial condition

$$g^{(i)}(0) = U/\pi v_F = 4\tilde{U} > 0, \tag{5.6}$$

the scaling equations lead to the fixed point

$$g^{(1)*} = 0,\ g^{(2)*} = 2\tilde{U}. \tag{5.7}$$

The fixed point characterizes the Tomonaga-Luttinger liquid (TL) phase. Since $g^{(1)}$ monotonically decreases, $g^{(1)3}$ terms in (5.4) and (5.5) are not essential for the scaling property so that we can drop them. Then we obtain

$$g^{(1)}(l) = \frac{4\tilde{U}}{1+4\tilde{U}l}, \tag{5.8}$$

$$g^{(2)}(l) = 2\tilde{U} + \frac{2\tilde{U}}{1+4\tilde{U}l}. \tag{5.9}$$

The TL phase is different from the SGM phase of the Hubbard ladder in that it belongs to the *weak-coupling universality class* and is *gapless*. Reflecting the weak-coupling nature, the intrachain self-energy effects are much weaker than in the ladder system. Consequently the strong suppression of the interchain one-particle process which is characteristic of the coupled ladders never occurs in the coupled chains. Furthermore, since the TL phase is gapless, the interchain two-particle hopping amplitude is ill defined (see the discussion given in §2).

The scaling equation for the interchain one-particle hopping amplitude, $t_{\rm chain\perp}$, [42] is, instead of (3.25), written as

$$\frac{d\ln t_{\rm chain\perp}(l)}{dl} = 1 - z_{\rm chain\parallel}(l), \tag{5.10}$$

with

$$z_{\rm chain\parallel}(l) = \frac{1}{4}\left[g^{(1)}(l)^2 + g^{(2)}(l)^2 - g^{(1)}(l)g^{(2)}(l)\right]. \tag{5.11}$$

Using (5.8) and (5.9), we obtain

$$\tilde{t}_{\rm chain\perp}(l) = \tilde{t}_{\rm chain\perp 0}\exp\left[(1-\tilde{U}^2)l + \frac{3\tilde{U}}{4}\left(\frac{1}{1+4\tilde{U}l} - 1\right)\right]. \tag{5.12}$$

Thus, contrary to the coupled-ladder case, $t_\perp$ becomes *relevant* for weak repulsion, $\tilde{U} < 1$, where the PRG scheme is reliable. We show this situation in the upper half plane of Fig.16, where the scaling flows of $t_{\rm chain\perp}(l)$ are shown for different $\tilde{U} = 0.1,\ 0.2,\ 0.3$ with $\tilde{t}_{\rm chain\perp 0} = 0.01$. The one-particle crossover temperature is defined by $\tilde{T}^{\rm chain}_{\rm cross} = e^{-l^{\rm chain}_{\rm cross}}$, where $l^{\rm chain}_{\rm cross}$ is determined by $\tilde{t}_{\rm chain\perp}(l^{\rm chain}_{\rm cross}) = 1$. [42] The scaling behavior of $\tilde{t}_{\rm chain\perp}(l)$ is also expressed in terms of the anomalous exponent, θ, as $\tilde{t}_{\rm chain\perp}(l) = \tilde{t}_{\rm chain\perp 0}\exp[(1-\theta)l]$ which gives $T^{\rm chain}_{\rm cross} = E_0[t_{\rm chain\perp 0}/E_0]^{1/(1-\theta)}$. The exact solution [51, 52, 53] tells us θ satisfies $\theta \le 1/8$, which again indicates $t_\perp$ is always relevant.

Structures of the leading-order scaling equations for V^M (M =CDW, SDW, SS, TS) are the same as those shown in Fig. 8, which give [42]

$$\frac{dV^{\rm DW}(l)}{dl} = \frac{1}{2}\left[\tilde{t}_{\rm chain\perp}(l)g^{\rm DW}(l)\right]^2\cos q_\perp + \frac{1}{2}g^{\rm DW}(l)V^{\rm DW}(l) - \frac{1}{4}V^{\rm DW}(l)^2, \tag{5.13}$$

for DW=CDW or SDW and

$$\frac{dV^{\rm S}(l)}{dl} = -\frac{1}{2}\left[\tilde{t}_{\rm chain\perp}(l)g^{\rm S}(l)\right]^2\cos q_\perp + \frac{1}{2}g^{\rm S}(l)V^{\rm S}(l) - \frac{1}{4}V^{\rm S}(l)^2, \tag{5.14}$$

for S=SS or TS. We put $q_\perp = 0$ and $q_\perp = \pi$ for the superconducting and density-wave channels, respectively. Coupling strengths of the corresponding composite particles are given by

$$\begin{cases} g^{\rm CDW}(l) = g^{(2)}(l) - 2g^{(1)}(l), \quad g^{\rm SDW}(l) = g^{(2)}(l), \\ g^{\rm SS}(l) = -(g^{(1)}(l) + g^{(2)}(l)), \quad g^{\rm TS}(l) = g^{(1)}(l) - g^{(2)}(l). \end{cases} \tag{5.15}$$

In the lower half plane of Fig. 16, we show the scaling flows of $V^{\rm SDW}$.

In Figs.17(a) and (b), we show the phase diagrams of the weakly coupled chains for $\tilde{U} = 0.3$ and for $\tilde{t}_{\rm chain\perp 0} = 0.01$, which correspond to Figs.11 and 12 in the weakly coupled ladders, respectively. For small $\tilde{U}$ and $\tilde{t}_{\rm chain\perp 0}$, where the PRG scheme is reliable, the system always undergoes a crossover to a two-dimensional phase (2D phase) via the one-particle processes. We show in Fig.17 for guidance the temperature, $\tilde{T}_{\rm SDW}$, at which $V^{\rm SDW}$ diverges.

For the reasons already stated in §4.1, it needs care to identify the finite temperature phase above $T_{\rm cross}^{\rm chain}$. We can identify it with the TL phase characterized by the fixed point (5.7) only for very small $\tilde{t}_{\rm chain\perp 0}$ or large $\tilde{U}$, where the one-particle crossover occurs at a very low temperature scale. For large $\tilde{t}_{\rm chain\perp 0}$ or small $\tilde{U}$, the one-particle crossover occurs at a very early stage of the scaling where the intrachain scattering processes are still far away from their fixed point corresponding to the low-energy asymptotics of the system. The ambiguity in regarding the phase at $T > T_{\rm cross}^{\rm chain}$ as the TL phase has some relevance to well known objections against the PRG approach to the present problem, as first emphasized by Anderson. [54] He stressed that it is crucial to treat the intrachain interaction exactly *before* switching on the interchain one-particle hopping. The PRG scheme misses this point, since we there treat the interaction and the interchain one-particle hopping, *on equal footing*, as perturbations to the *one-dimeniosnal free fermion system*. Along Anderson's claim, by using the exact propagator of the TL liquid and calculating the momentum distribution function, Castellani *et al.* [55] demonstrated that the TL phases are unstable with respect to arbitrary small interchain one-particle hopping, even if the interaction is strong. Their conclusion supports the results obtained through the PRG scheme, contraly to the expectation of Anderson.

On the other hand, the effects of the interchain one-particle hopping have been studied in view of "coherence" or "incoherence" rather than its "relevance" or "irrelevance". [56, 57] With the aid of the knowledge of the two-level system, it was demonstrated [56] that there exists a critical value of the inter-Luttinger-liquid hopping below which there is no coherent one-particle hopping between the liquids, which contradicts to the PRG results. At present, however, it remains an unsettled question whether the TL phase is stable against the interchain one-particle hopping or not.

§6. Concluding Remarks

In the present paper we applied the perturbative renormalization group (PRG) method to discuss dimensional crossovers in Hubbard ladders coupled via weak interladder one-particle hopping, $t_\perp$. We set up and solved the scaling equations for the interladder one-particle and two-particle hopping amplitudes by treating the intraladder interactions and the interladder one-particle hopping as perturbations to the free electron system on the isolated ladders. We found that *the scaling flow toward the spin gap metal phase (SGM phase) in the isolated Hubbard ladder strongly suppresses the interladder one-particle process and consequently, for any finite intraladder Hubbard repulsion, $U > 0$, there exits a finite crossover value of the interladder one-particle hopping, $t_{\perp c}$.*

For $0 < t_\perp < t_{\perp c}$, the bulk d-wave superconducting phase is stabilized via the condensation of bipolarons, where interladder Josephson tunnleling of bipolarons occur. The superconducting transition occurs at the low temperature scales where the intraladder scattering processes nearly

attain their strong coupling values (see Fig.10), which suggests the spin gap is already well developed around the temperature region. For $t_{\perp c} < t_\perp$, the system undergoes the crossover from the spin gap metal phase to the two-dimensional phase (2D phase) where the interladder one-particle hopping becomes coherent and one-dimensionality of the isolated ladder is completely lost. The temperature scales of the one-particle crossover is, however, not low enough to ensure a well-developed spin gap (see Fig.10), since the one-particle crossover occurs at an early stage of scaling, where the intraladder system does not approach the strong coupling region as yet. Thus it is disputable whether we can assign the region $T > T_{\rm cross}$ to the SGM phase or not.

Our results are best summarized in the $t_\perp$-T phase diagram, Fig.11. Roughly speaking, we may regard increasing $t_\perp$ as applying pressure. In the doped spin ladder, $Sr_{2.5}Ca_{11.5}Cu_{24}O_{41}$, the superconductivity sets in below 10 K under 3.5 GPa $\sim$ 8 GPa. The observed transition temperature, $T_c^{\rm obs}$, increases with the pressure and reaches the maximum 6K around the optimal pressure $P_{\rm opt} \sim$ 4.5 GPa. [12] Our result in Fig.11 qualitatively reproduces the increase of $T_c^{\rm obs}$ for $P < P_{\rm opt}$. For $P > P_{\rm opt}$, the $T_c^{\rm obs}$ gradually decreases and the resistivity along the ladder, ρ_c, shows gradual change from T-linear to T^2-dependence with increasing the applied pressure. [12] This fact strongly suggests that for $P > P_{\rm opt}$ the system is regarded as an anisotropic 2D Fermi liquid. In our scheme, the existence of $\tilde{t}_{\perp c}$ would correspond to the existence of $P_{\rm opt}$. As was suggested in section 4.4, it is reasonable to suppose that in the 2D phase a superconducting instability via Suhl-Kondo mechanism [47] becomes possible due to the interband exchange-like interaction which is strongly enhanced by an *interband nesting*. Then the applied pressure tends to decrease the degree of the interband nesting and consequently the transition temperature should decrease with increasing the applied pressure.

We also discussed difference between dimensional crossovers in weakly coupled Hubbard chains and ladders within the framework of the PRG. The difference originates from different universality classes to which the corresponding isolated systems belong. The isolated Hubbard chain belongs to the weak coupling Tomonaga-Luttinger liquid phase which is gapless, while the isolated Hubbard ladder belongs to the strong coupling phase with the spin gap. In the former case, the two-particle process is always dominated by the one-particle process, unless we assume very large intrachain Hubbard repulsion which is out of the perturbative scheme. On the contrary, in the latter case, the one-particle processes are strongly suppressed through growth of the intraladder scattering processes which lead the isolated Hubbard ladder toward the spin gap metal phase. Consequently when $t_\perp$ sets in, there exists, for any finite intraladder Hubbard repulsion, the region where the two-particle crossover dominates the one-particle crossover.

Acknowledgements

J.K was supported by a Grant-in-Aid for Encouragement for Young Scientists from the Ministry of Education, Science, Sports and Culture, Japan.

Appendix A: Derivation of the Scaling Equations

The PRG program takes three steps: 1. coarse graining, 2. field rescaling and 3. renormalization.

Coarse Graining

As depicted in Fig. 18, first we divide the linearized intraladder bands with scaling-dependent bandwidth $E(l) = E_0 e^{-l}$ into the inner region, $\mathcal{C}_{\nu m<}$ (slow modes), and the outer shell, $d\mathcal{C}_{\nu m>}$ (fast modes), where

$$\mathcal{C}_{\nu m<} \equiv \left\{ k_\parallel \mid\mid \varepsilon_{\nu m}(k_\parallel) \mid < E(l+dl)/2 \right\},$$
$$d\mathcal{C}_{\nu m>} \equiv \left\{ k_\parallel \mid E(l+dl)/2 < \mid \varepsilon_{\nu m}(k_\parallel) \mid < E(l)/2 \right\}.$$

Coarse graining means integration of the fermion degrees of freedom over $d\mathcal{C}_{\nu m>}$ with thickness

$$\mid dE(l) \mid = \frac{1}{2}E(l)dl. \tag{A·1}$$

We leave ε_n and $k_\perp$ free. This procedure is performed for each branch ($\nu m = LB, LA, RA, RB$) and spin.

The action (3.1) is then decomposed into the slow and the fast counterparts as

$$\begin{aligned} S &= S_< + S_> \\ &= S^{(1)}_{\parallel<} + S^{(2)}_{\parallel<} + S^{(1)}_{\perp<} + S^{(2)}_{\perp<} + S^{(1)}_{\parallel>} + S^{(2)}_{\parallel>} + S^{(1)}_{\perp>} + S^{(2)}_{\perp>}, \end{aligned}$$

where $S_<$ consists of only the modes in $\mathcal{C}_{\nu m<}$, while $S_>$ includes the modes in $d\mathcal{C}_{\nu m>}$. The partition function is then rewritten as

$$Z = \int \mathcal{D}_< \exp\left[S^{(1)}_{\parallel<} + S^{(2)}_{\parallel<} + S^{(1)}_{\perp<} + S^{(2)}_{\perp<}\right] \int \mathcal{D}_> \exp\left[S^{(1)}_{\parallel>} + S^{(2)}_{\parallel>} + S^{(1)}_{\perp>} + S^{(2)}_{\perp>}\right],$$

where $\mathcal{D}_<$ and $\mathcal{D}_>$ symbolize the measure over the modes in $C_{\nu m<}$ and $d\mathcal{C}_{\nu m>}$, respectively. Under the weak coupling condition, $t_\perp, g^{(i)}_\mu \ll t, t'$, we expand $\exp\left[S^{(1)}_{\parallel>} + S^{(2)}_{\parallel>} + S^{(1)}_{\perp>} + S^{(2)}_{\perp>}\right]$ with regard to $S^{(2)}_{\parallel>}$, $S^{(1)}_{\perp>}$, and $S^{(2)}_{\perp>}$, and integrate out the modes in $d\mathcal{C}_>$. Then we obtain

$$Z = \int \mathcal{D}_< \exp\left[S^{(1)}_{\parallel<} + S^{(2)}_{\parallel<} + S^{(1)}_{\perp<} + S^{(2)}_{\perp<} + \sum_{l,m,n=0}^{\infty} \Gamma_{lmn}\right],$$

where

$$\Gamma_{lmn} = \frac{1}{l!m!n!} \langle\!\langle \left[S^{(2)}_{\parallel>}\right]^l \left[S^{(1)}_{\perp>}\right]^m \left[S^{(2)}_{\perp>}\right]^n \rangle\!\rangle_{\rm c}, \tag{A·2}$$

$\langle\!\langle (\cdots) \rangle\!\rangle = \int \mathcal{D}_> e^{S^{(1)}_{\parallel>}} (\cdots)$ and the subscript 'c' represents the connected diagram. Now we obtain the modified action, $\bar{S}_<$, with the modified intraladder propagators and interladder one- and two-particle hopping amplitudes written as

$$\bar{\mathcal{G}}^{-1}_{\nu m}(K_\parallel) = [1 + z_\parallel(l)dl + \mathcal{O}(dl^2)]\mathcal{G}^{-1}_{\nu m}(K), \tag{A·3}$$

$$\bar{t}_\perp = [1 + \mathcal{O}(dl^2)]t_\perp, \tag{A·4}$$

$$\bar{g}^{(i)}_\mu = [1 + z^{(i)}_{\parallel\mu}(l)dl + \mathcal{O}(dl^2)]g^{(i)}_\mu, \tag{A·5}$$

$$\bar{V}^M_\mu = f^M_\mu(l)dl + [z^M_{\perp\mu}(l)dl + \mathcal{O}(dl^2)]V^M_\mu, \tag{A·6}$$

where f^M_μ symbolizes the generator of V^M_μ which is diagramatically shown in Fig. 7. In the low order arguments, $z^M_{\perp\mu}$ has $[V^M_\mu]^n$ contributions with $n = 0$ and $n = 1$.

We obtain the $z_\parallel(l)$, $z^{(i)}_{\parallel\mu}(l)$, $f^M_\mu(l)$ and $z^M_{\perp\mu}(l)$, by picking up and evaluating the Feynmann diagrams which give contributions in proportion to dl. The diagrams in Figs.4(a) and 4(b) give $z^{(1)}_{\parallel\mu}(l)$ and $z^{(2)}_{\parallel\mu}(l)$, respectively, which come from $\Gamma_{200} + \Gamma_{300}$. The diagrams in Fig.4(c) give $z_\parallel(l)$ which come from Γ_{200}. The diagrams in Fig.7 give f^M_μ which come from Γ_{220}. The second and third diagrams on the r.h.s of Fig.8 give $z^M_{\perp\mu}$ which come from $\Gamma_{101} + \Gamma_{002}$.

Field Rescaling

The right-moving sector of the coarse-grained intraladder kinetic action is

$$\sum_{{\rm i}\varepsilon_n} \sum_\sigma \int_{-E(l+dl)/2v_F}^{E(l+dl)/2v_F} \frac{dk_\parallel}{2\pi} [1 + z_\parallel(l)dl] \mathcal{G}^{-1}_{Rm}(K_\parallel) R^*_{m\sigma}(K) R_{m\sigma}(K). \tag{A·7}$$

To restore the original cutoff and leave the intraladder kinetic action, $S_\parallel$, invariant, we tune the momenta, frequencies and field variables as

$$\begin{cases} \bar{K}_\parallel = e^{dl} K_\parallel = (1+dl)\, K_\parallel, \\ \bar{R}_{m\sigma}(\bar{K}) = [1 + \frac{1}{2}\{z_\parallel(l) - 3\} dl] R_{m\sigma}(K), \end{cases}$$

where

$$\begin{cases} \bar{K}_\parallel = (e^{dl} k_\parallel, \mathrm{i} e^{dl} \varepsilon_n), \\ \bar{K} = (e^{dl} k_\parallel, k_\perp, \mathrm{i} e^{dl} \varepsilon_n). \end{cases}$$

We must leave the transverse momentum, $k_\perp$, unchanged since the scaling law is well defined only along the longitudinal direction. Then we see that (A·7) becomes

$$\sum_{\mathrm{i}\bar{\varepsilon}_n} \sum_\sigma \int_{-E(l)/2v_F}^{E(l)/2v_F} \frac{d\bar{k}_\parallel}{2\pi} \mathcal{G}_{Rm}^{-1}(\bar{K}_\parallel) \bar{R}^*_{m\sigma}(\bar{K}) \bar{R}_{m\sigma}(\bar{K}),$$

which is just the same form as the initial one, namely, scale-invariant.

Renormalization

Finally we renormalize the physical quantities in the action and set up the differential equations for them with keeping $S_\parallel$ scale-invariant. Discarding all the $O(dl^2)$ terms in (A·3)-(A·6) and taking account of (A·6) and (A·8), we obtain the scaling equations

$$\frac{d \ln g_\mu^{(i)}(l)}{dl} = z_{\parallel\mu}^{(i)}(l) - 2 z_\parallel(l), \tag{A·8}$$

$$\frac{d \ln t_\perp(l)}{dl} = 1 - z_\parallel(l), \tag{A·9}$$

$$\frac{dV_\mu^M(l)}{dl} = f_\mu^M(l) + z_\mu^M(l) V_\mu^M(l), \tag{A·10}$$

which give (3.9), (3.25) and (3.29), respectively. Note that $z_{\perp\mu}^M$ has $[V_\mu^M]^n$ contributions with $n = 0$ and $n = 1$.

Appendix B: Evaluation of Self-Energy Diagrams

We here give in detail the derivation of the factor, $z_\parallel$, which governs the one-dimensional crossover. In Ref.[13], the same results are given. The factor, $z_\parallel$, comes from the renormalization of the intraladder propagotor, $\mathcal{G}_{\nu m}(K_\parallel)$. ($\nu = R,\, L:\ m = A, B$). Since $z_\parallel$ is independent of ν and m, we consider only the case of $\mathcal{G}_{RB}(K_\parallel)$.

The 2nd order renomalization of $\mathcal{G}_{\nu m}(K_\parallel)$ originates from $\Gamma_{200} = \frac{1}{2}\langle\langle \left[S_{\parallel>}^{(2)}\right]^2 \rangle\rangle$. In Fig.19, we give diagrammatic representations for Γ_{200} which renoremalize $\mathcal{G}_{RB}(K_\parallel)$. Although there are a lot of ways to assign the outer-shell mode in $S_\parallel^{(2)}$, there are only two possible ways which renormalize $\mathcal{G}_{\nu m}(K_\parallel)$. We specify these two cases by arrows in Fig.19:

$$\begin{cases} \mathrm{case-I}: \ \ k'_\parallel \in d\mathcal{C}_{Lm_1>},\ k'_\parallel + q_\parallel \in \mathcal{C}_{Lm_2<},\ k_\parallel - q_\parallel \in \mathcal{C}_{Rm_3<}, \\ \mathrm{case-II}: \ \ k'_\parallel \in \mathcal{C}_{Rm_1<},\ k'_\parallel + q_\parallel \in d\mathcal{C}_{Lm_2>},\ k_\parallel - q_\parallel \in \mathcal{C}_{Rm_3<}. \end{cases}$$

Then, among a lot of terms included in Γ_{200}, the contribution to the renormalization of $\mathcal{G}_{RB}(k_\parallel)$ is obtained as

$$\Gamma_{200}^{\mathrm{S.E}} = 2\,(2\pi v_F)^2 \Big[(g_0^{(1)^2} + g_0^{(2)^2} - g_0^{(1)} g_0^{(2)}) \mathcal{I}^{BBB}(dl)$$

$$+{g_f^{(1)}}^2\mathcal{I}^{BAA}(dl)+{g_f^{(2)}}^2\mathcal{I}^{AAB}(dl)-g_f^{(1)}g_f^{(2)}\mathcal{I}^{AAB}(dl)$$
$$+{g_t^{(1)}}^2\mathcal{I}^{AAB}(dl)+{g_t^{(2)}}^2\mathcal{I}^{BAA}(dl)-g_t^{(1)}g_t^{(2)}\mathcal{I}^{BAA}(dl)\Big],$$

where

$$\mathcal{I}^{m_1m_2m_3}(dl)=\mathcal{I}_{\rm I}^{m_1m_2m_3}(dl)+\mathcal{I}_{\rm II}^{m_1m_2m_3}(dl)$$

with $\mathcal{I}_{\rm I}^{m_1m_2m_3}(dl)$ and $\mathcal{I}_{\rm II}^{m_1m_2m_3}(dl)$ corresponding to the cases I and II, respectively. $\mathcal{I}_{\rm I}^{m_1m_2m_3}(dl)$ is evaluated as

$$\mathcal{I}_{\rm I}^{m_1m_2m_3}(dl)=T^2\int_{dC_{Lm_1>}}\frac{dk'_\parallel}{2\pi}\int\frac{dq}{2\pi}\sum_{m,l}\mathcal{G}_{Lm_1}(k',{\rm i}\varepsilon'_m)\mathcal{G}_{Rm_2}(k-q,{\rm i}\varepsilon_n-{\rm i}\omega_l)\mathcal{G}_{Lm_3}(k'+q,{\rm i}\varepsilon'_m+{\rm i}\omega_l)$$
$$=-\frac{1}{4}\int_{dC_{Lm_1>}}\frac{d\varepsilon'_{Lm_1}}{2\pi v_F}\int\frac{dq}{2\pi}\frac{\mathcal{T}(\varepsilon'_{Lm_1},k,q;T)}{D+2v_F(q-\Delta k_F)},$$

where $\Delta k_F=k_{Fm_1}-k_{Fm_2}$ and $D={\rm i}\varepsilon_n-v_F(k-k_{FB})$. The thermal factor is given by

$$\mathcal{T}(\varepsilon_{Lm_1},K,q;T)=$$
$$\left[\tanh\frac{\varepsilon_{Lm_1}}{2T}-\tanh\frac{\varepsilon_{Lm_1}+v_F(\Delta k_F-q)}{2T}\right]\left[\coth\frac{v_F(q-\Delta k_F)}{2T}-\tanh\frac{v_F(k-k_{FB}-q+\Delta k_F)}{2T}\right].$$

In the low-temperature limit,

$$\mathcal{T}(\varepsilon_{Lm_1},k,q;T=0)=\begin{cases}4 & \text{for}\quad \varepsilon_{Lm_1}\left[\varepsilon_{Lm_1}+v_F(\Delta k_F-q)\right]<0,\\ 0 & \text{for}\quad \varepsilon_{Lm_1}\left[\varepsilon_{Lm_1}+v_F(\Delta k_F-q)\right]>0.\end{cases}$$

Taking account of the restriction on available $q_\parallel$, coming from the case-I condition, we obtain

$$\mathcal{I}_{\rm I}^{m_1m_2m_3}(dl)=-\frac{1}{4\pi^2v_F}\left[\int_{\frac{E_0-|dE_0(l)|}{2}}^{\frac{E_0}{2}}d\varepsilon'_{Lm_1}\int_{\frac{E_0}{2v_F}+\Delta k_F}^{\frac{E_0}{v_F}+\Delta k_F}dq+\int_{\frac{-E_0}{2}}^{-\frac{E_0-|dE_0(l)|}{2}}d\varepsilon'_{Lm_1}\int_{-\frac{E_0}{v_F}+\Delta k_F}^{-\frac{E_0}{2v_F}+\Delta k_F}dq\right]$$
$$\frac{1}{D+2v_F(q-\Delta k_F)}$$
$$==-\frac{|\,dE_0(l)\,|}{16\pi^2v_F^2}\ln\frac{[E_0-D]\,[2E_0+D]}{[E_0+D]\,[2E_0-D]}.$$

By taking the limit $D/E_0\ll 1$, we obtain

$$\mathcal{I}_{\rm I}^{m_1m_2m_3}(dl)=\frac{D}{16\pi^2v_F^2}dl=\frac{1}{16\pi^2v_F^2}\mathcal{G}_{RB}^{-1}(K)dl.$$

Evaluation of $\mathcal{I}_{\rm II}^{m_1m_2m_3}(dl)$ gives the same result. Thus we obtain

$$\Gamma_{200}^{\rm S.E}=z_\parallel\mathcal{G}_{RB}^{-1}(K)dl,$$

and the modified intraladder one-particle action

$$\bar{S}_\parallel^{(1)}=\sum_K\sum_{m=A,B}\sum_\sigma(1+z_\parallel dl)\left[\mathcal{G}_{Lm}^{-1}(K_\parallel)L_{m\sigma}^*(K)L_{m\sigma}(K)+\mathcal{G}_{Rm}^{-1}(K_\parallel)R_{m\sigma}^*(K)R_{m\sigma}(K)\right],$$

where $z_\parallel$ is given by (3.10). This result leads to (A·3).

Appendix C: Evaluation of Generators for Interladder Two-Particle Hopping Processes

We here give a full account of evaluation of the generators for the two-particle hopping processes, f_μ^M. It is convenient to rewrite the intraladder interaction part in terms of the composite particle variables as

$$\begin{aligned} S_{\rm int} = \frac{\pi v_F}{2}\sum_{Q_\parallel}\Big[& g_0^{\rm CDW}\mathcal{O}^{BB*}_{\rm CDW}\mathcal{O}^{BB}_{\rm CDW} + g_t^{\rm CDW}\mathcal{O}^{BA*}_{\rm CDW}\mathcal{O}^{AB}_{\rm CDW} + g_f^{\rm CDW}\mathcal{O}^{BA*}_{\rm CDW}\mathcal{O}^{BA}_{\rm CDW} \\ & + g_0^{\rm SDW}\vec{\mathcal{O}}^{BB*}_{\rm SDW}\cdot\vec{\mathcal{O}}^{BB}_{\rm SDW} + g_t^{\rm SDW}\vec{\mathcal{O}}^{BA*}_{\rm SDW}\cdot\vec{\mathcal{O}}^{AB}_{\rm SDW} + g_f^{\rm SDW}\vec{\mathcal{O}}^{BA*}_{\rm SDW}\cdot\vec{\mathcal{O}}^{BA}_{\rm SDW} \\ & + g_0^{\rm SS}\mathcal{O}^{BB*}_{\rm SS}\mathcal{O}^{BB}_{\rm SS} + g_t^{\rm SS}\mathcal{O}^{BB*}_{\rm SS}\mathcal{O}^{AA}_{\rm SS} + g_f^{\rm SS}\mathcal{O}^{AB*}_{\rm SS}\mathcal{O}^{AB}_{\rm SS} \\ & + g_0^{\rm TS}\vec{\mathcal{O}}^{BB*}_{\rm TS}\cdot\vec{\mathcal{O}}^{BB}_{\rm TS} + g_t^{\rm TS}\vec{\mathcal{O}}^{BB*}_{\rm TS}\cdot\vec{\mathcal{O}}^{AA}_{\rm TS} + g_f^{\rm TS}\vec{\mathcal{O}}^{AB*}_{\rm TS}\cdot\vec{\mathcal{O}}^{AB}_{\rm TS}\Big] + (A\leftrightarrow B), \end{aligned} \tag{C·1}$$

where $\mathcal{O}_M^{m_1m_2}$ denotes $\mathcal{O}_M^{m_1m_2}(Q_\parallel)$.

As an illustration, we derive the generator for the CDW channel, $f_\mu^{\rm CDW}$. In the action, (C·2), the CDW channel consists of

$$\begin{aligned} S_{\rm int}^{\rm CDW} = & \frac{1}{2}\pi v_F g_0^{\rm CDW}\sum_{Q_\parallel}\mathcal{O}^{BB*}_{\rm CDW}(Q_\parallel)\mathcal{O}^{BB}_{\rm CDW}(Q_\parallel) \\ & + \frac{1}{2}\pi v_F\sum_{Q_\parallel}\Big[g_t^{\rm CDW}\mathcal{O}^{BA*}_{\rm CDW}(Q_\parallel)\mathcal{O}^{AB}_{\rm CDW}(Q_\parallel) + g_f^{\rm CDW}\mathcal{O}^{BA*}_{\rm CDW}(Q_\parallel)\mathcal{O}^{BA}_{\rm CDW}(Q_\parallel)\Big] + (A\leftrightarrow B). \end{aligned}$$

The generators depicted in Fig. 7(a) come from Γ_{022}. Among a lot of terms included in Γ_{220}, the contribution to $f_\mu^{\rm CDW}$, $\Gamma_{220}^{\rm CDW}$, is obtained by assigning composite field variables to the outer shell mode as

$$\begin{aligned} S^{\rm CDW}_{\rm int>} = & \frac{1}{2}\pi v_F g_0^{\rm CDW}\textstyle\sum_{Q_\parallel}(\mathcal{O}^{BB*}_{\rm CDW>}\mathcal{O}^{BB}_{\rm CDW<} + \mathcal{O}^{BB*}_{\rm CDW<}\mathcal{O}^{BB}_{\rm CDW>} + \mathcal{O}^{AA*}_{\rm CDW>}\mathcal{O}^{AA}_{\rm CDW<} + \mathcal{O}^{AA*}_{\rm CDW<}\mathcal{O}^{AA}_{\rm CDW>}) \\ & + \frac{1}{2}\pi v_F\textstyle\sum_{Q_\parallel}[g_t^{\rm CDW}(\mathcal{O}^{BA*}_{\rm CDW>}\mathcal{O}^{AB}_{\rm CDW<} + \mathcal{O}^{BA*}_{\rm CDW<}\mathcal{O}^{AB}_{\rm CDW>} + \mathcal{O}^{AB*}_{\rm CDW>}\mathcal{O}^{BA}_{\rm CDW<} + \mathcal{O}^{AB*}_{\rm CDW<}\mathcal{O}^{BA}_{\rm CDW>}) \\ & + g_f^{\rm CDW}(\mathcal{O}^{BA*}_{\rm CDW>}\mathcal{O}^{BA}_{\rm CDW<} + \mathcal{O}^{BA*}_{\rm CDW<}\mathcal{O}^{BA}_{\rm CDW>} + \mathcal{O}^{AB*}_{\rm CDW>}\mathcal{O}^{AB}_{\rm CDW<} + \mathcal{O}^{AB*}_{\rm CDW<}\mathcal{O}^{AB}_{\rm CDW>})] \\ & + (A\leftrightarrow B), \end{aligned}$$

where

$$\begin{aligned} \mathcal{O}^{mm'}_{\rm CDW<} &= \beta^{-1/2}\sum_{k_\parallel+q_\parallel\in\mathcal{C}_{Rm<}}\sum_{k_\parallel\in\mathcal{C}_{Lm<}}\sum_{{\rm i}\varepsilon_n}\sum_\sigma R^*_{m\sigma}(K_\parallel+Q_\parallel)L_{m'\sigma}(K_\parallel), \\ \mathcal{O}^{mm'}_{\rm CDW>} &= \beta^{-1/2}\sum_{k_\parallel+q_\parallel\in d\mathcal{C}_{Rm>}}\sum_{k_\parallel\in d\mathcal{C}_{Lm>}}\sum_{{\rm i}\varepsilon_n}\sum_\sigma R^*_{m\sigma}(K_\parallel+Q_\parallel)L_{m'\sigma}(K_\parallel). \end{aligned}$$

Then we obtain

$$\begin{aligned} \Gamma_{220}^{\rm CDW} &= \frac{1}{4}\langle\langle S^2_{\perp>}\{S^{\rm CDW}_{\rm int>}\}^2\rangle\rangle \\ &= \frac{\pi^2v_F^2}{8}(g_0^{\rm CDW})^2\sum_Q\langle\langle S^2_{\perp>}\mathcal{O}^{BB*}_{\rm CDW>}O^{BB}_{\rm CDW>}\rangle\rangle\mathcal{O}^{BB*}_{\rm CDW<}\mathcal{O}^{BB}_{\rm CDW<} \\ &+ \frac{\pi^2v_F^2}{8}\sum_Q\Big[(g_t^{\rm CDW})^2\langle\langle S^2_{\perp>}\mathcal{O}^{AB*}_{\rm CDW>}\mathcal{O}^{AB}_{\rm CDW>}\rangle\rangle + (g_f^{\rm CDW})^2\langle\langle S^2_{\perp>}\mathcal{O}^{BA*}_{\rm CDW>}\mathcal{O}^{BA}_{\rm CDW>}\rangle\rangle\Big]\mathcal{O}^{BA*}_{\rm CDW<}\mathcal{O}^{BA}_{\rm CDW<} \\ &+ \frac{\pi^2v_F^2}{4}g_t^{\rm CDW}g_f^{\rm CDW}\sum_Q\langle\langle S^2_{\perp>}\mathcal{O}^{AB*}_{\rm CDW>}\mathcal{O}^{AB}_{\rm CDW>}\rangle\rangle\mathcal{O}^{BA*}_{\rm CDW<}\mathcal{O}^{AB}_{\rm CDW<} + (A\leftrightarrow B), \end{aligned}$$

where the first, second and third lines on the r.h.s of the second equation correspond to the first, second and third lines of Fig. 7(a). We obtain, in the low temperature limit,

$$\langle\langle \mathcal{O}^{mm}_{\rm CDW>} S^2_\perp \mathcal{O}^{mm*}_{\rm CDW>}\rangle\rangle = -t_\perp^2 \cos(q_\perp) T \sum_{k_\parallel \in d\mathcal{C}_{Rm>}} \sum_{\varepsilon_n} G^2_{Lm}(k_\parallel - 2k_{Fm}, {\rm i}\varepsilon_n) G^2_{Rm}(k_\parallel, {\rm i}\varepsilon_n)$$

$$= \frac{1}{2\pi v_F} t_\perp^2 \cos(q_\perp d_\perp) \left[\int_{-\frac{E_0(l)}{2}}^{-\frac{E_0(l)-|dE_0(l)|}{2}} + \int_{\frac{E_0(l)-|dE_0(l)|}{2}}^{\frac{E_0(l)}{2}} \right] d\varepsilon_{Rm} \left[\frac{\frac{\beta}{2} \coth^{-2} \frac{\beta\varepsilon_{RB}}{2}}{(-2\varepsilon_{RB})^2} + \frac{2\tanh\frac{\beta\varepsilon_R}{2}}{(-2\varepsilon_{RB})^3} \right]$$

$$= -\frac{t_\perp^2 dl}{\pi v_F} E_0^{-2}(l) \cos q_\perp .$$

Similar manipulation gives

$$\langle\langle \mathcal{O}^{m\bar{m}}_{\rm DW} S^2_\perp \mathcal{O}^{m\bar{m}*}_{\rm DW}\rangle\rangle = +\frac{t_\perp^2 dl}{\pi v_F} E_0^{-2}(l) \cos q_\perp ,$$

where m and $\bar{m}$ denote different bands. Thus we obtain

$$\begin{aligned}
\Gamma^{\rm CDW}_{220} = & -\frac{t_\perp^2 \pi v_F}{8E_0^2(l)} dl (g_0^{\rm CDW})^2 \sum_Q \cos q_\perp \mathcal{O}^{BB*}_{\rm CDW<} \mathcal{O}^{BB}_{\rm CDW<} \\
& + \frac{t_\perp^2 \pi v_F}{8E_0^2(l)} dl \left[(g_t^{\rm CDW})^2 + (g_f^{\rm CDW})^2 \right] \sum_{Q_\parallel} \cos q_\perp \mathcal{O}^{BA*}_{\rm CDW<} \mathcal{O}^{BA}_{\rm CDW<} \\
& + \frac{t_\perp^2 \pi v_F}{4E_0^2(l)} dl g_t^{\rm CDW} g_f^{\rm CDW} \sum_{Q_\parallel} \cos q_\perp \mathcal{O}^{BA*}_{\rm CDW<} \mathcal{O}^{AB}_{\rm CDW<} .
\end{aligned}$$

After the field rescaling procedure, the first, second and third lines of the above equation give the first terms in (3.30), (3.32) and (3.33), respectively. It is here useful to present the following results.

$$\begin{aligned}
\langle\langle \mathcal{O}^{mm}_{\rm DW} S^2_\perp \mathcal{O}^{mm*}_{\rm DW}\rangle\rangle &= -\tfrac{t_\perp^2 dl}{\pi v_F} E_0^{-2}(l) \cos q_\perp , \\
\langle\langle \mathcal{O}^{m\bar{m}}_{\rm DW} S^2_\perp \mathcal{O}^{m\bar{m}*}_{\rm DW}\rangle\rangle &= +\tfrac{t_\perp^2 dl}{\pi v_F} E_0^{-2}(l) \cos q_\perp , \\
\langle\langle \mathcal{O}^{mm}_{\rm S} S^2_\perp \mathcal{O}^{mm*}_{\rm S}\rangle\rangle &= +\tfrac{t_\perp^2 dl}{\pi v_F} E_0^{-2}(l) \cos q_\perp , \\
\langle\langle \mathcal{O}^{m\bar{m}}_{\rm S} S^2_\perp \mathcal{O}^{m\bar{m}*}_{\rm S}\rangle\rangle &= -\tfrac{t_\perp^2 dl}{\pi v_F} E_0^{-2}(l) \cos q_\perp ,
\end{aligned}$$

where DW=CDW/SDW and S=SS/TS. When we evaluate the second and third diagrams of Figs.8(a) and 8(b), it is useful to note the outer shell integration, which appears in the evaluation of Γ_{011} and Γ_{002}, is given by

$$\langle\langle \mathcal{O}^{mm}_M \mathcal{O}^{mm*}_M\rangle\rangle = \langle\langle \mathcal{O}^{m\bar{m}}_M \mathcal{O}^{m\bar{m}*}_M\rangle\rangle = \frac{dl}{\pi v_F}$$

for M = CDW, SDW, SS or TS.

[1] E. Daggoto and T. M. Rice: Science **271** (1996) 618 and references therein.

[2] M. Uehara, T. Nagata, J. Akimitsu, H. Takahashi, N. Môri and K. Kinoshita: J. Phys. Soc. Jpn. **65** (1996) 2764.

[3] T. Osafune, M. Motoyama, H. Eisaki and S. Uchida: Phys. Rev. Lett. **78** (1997) 1980.

[4] Y. Mizuno, T. Tohyama and S. Maekawa: J. Phys. Soc. Jpn. **66** (1997) 937.

[5] N. Motoyama, T. Osafune, T. Kaneshita, H. Eisaki and S. Uchida: Phys. Rev.**B 55** (1997) R3386.

[6] S. Tsuji, K. Kumagai, M. Kato and Y. Koike: J. Phys. Soc. Jpn. **65** (1996) 3474.

[7] M. Takigawa: submitted to Phys. Rev.**B**.

[8] R. S. Eccleston, M. Azuma and M. Takano: Phys. Rev.**B 63** (1996) R14721.

[9] K. Kumagai, S. Tsuji, M. Kato and Y. Koike: Phys. Rev. Lett. **78** (1997) 1992.

[10] K. Magishi,*et.al*: submitted to Phys. Rev.**B**.

[11] M. Arai and H. Tsunetsugu: Phys. Rev.**B 56** (1997) 4305.

[12] J. Akimitsu,*et.al*: Physica **C282-287** (1997) 153. H. Takahashi, and N. Mori: Physica **C263** (1996) 475.

[13] M. Fabrizio: Phys. Rev.**B 48** (1993) 15838.

[14] A. M. Finkel'stein and A. I. Larkin: Phys. Rev.**B 47** (1993) 10461.

[15] D. V. Khveshchenko and T. M. Rice: Phys. Rev.**B 50** (1994) 252.

[16] L. Balents and M. P. A Fisher: Phys. Rev.**B 53** (1996) 12133.

[17] H. J. Schulz: Phys. Rev.**B53** (1996) 2959.

[18] A. A. Nersesyan, A. Luther and F. V. Kusmartsev: Phys. Lett. **A176** (1993) 363.

[19] H. Yoshioka and Y. Suzumura: J. Low. Temp. Phys. **106** (1997) 49.

[20] D. V. Khveshchenko: Phys. Rev.**B 50** (1994) 380.

[21] N. Nagaosa: Solid. State. Commun. **94** (1995) 495.

[22] D. G. Shelton and A. M. Tsvelik: Phys. Rev.**B 53** (1996) 14036.

[23] N. Nagaosa and M. Oshikawa: J. Phys. Soc. Jpn. **66** (1997) 937.

[24] H. Tsunetsugu, M. Troyer and T. M. Rice: Phys. Rev.**B 49** (1994) 16078.

[25] R. M. Noack, S. R. White and D. G. Scalapino: Phys. Rev. Lett. **73** (1994) 882.

[26] C. A. Hayward and D. Poilblanc: Phys. Rev.**B 53** (1996) 11721.

[27] K. Kuroki, T. Kimura and H. Aoki: Phys. Rev.**B 54** (1996) 15641.

[28] D. Poilblanc, D. J. Scalapino and W. Hanke: Phys. Rev.**B 52** (1995) 6796.

[29] K. Sano: J. Phys. Soc. Jpn. **65** (1996) 1146.

[30] H. Tsunetsugu, M. Troyer and T. M. Rice: Phys. Rev.**B 51** (1995) 16456.

[31] E. Orignac and T. Giamarchi:preprint (cond-mat/9704064).

[32] H-H. Lin, L. Balents and M. P. A Fisher: Phys. Rev.**B 56** (1997) 6569.

[33] J. Kishine and K. Yonemitsu:J. Phys. Soc. Jpn. **66** (1997) 3725.

[34] J. Sólyom: Adv. Phys. **28** (1979) 201.

[35] Yu. A. Firsov, V. N. Prigodin and Chr. Seidel: Phys. Rep. **126** (1985) 245.

[36] J. Voit: Rep. Prog. Phys. **58** (1995) 977.

[37] S. A. Brazovskii and V. M. Yakovenko: Sov. Phys. JETP **62** (1985) 1340.

[38] Y. Suzumura: J. Phys. Soc. Jpn. **54** (1985) 2386.

[39] V. M. Yakovenko: JETP Lett. **56** (1992) 510.

[40] C. Bourbonnais: Mol. Cryst. Liq. Cryst. **119** (1985)11.

[41] C. Bourbonnais and L. G. Caron: Physica **143BC** (1986) 450.

[42] C. Bourbonnais and L. G. Caron: Int. J. Mod. Phys. **B5** (1991) 1033.

[43] D. Boies, C. Bourbonnais and A. -M. S. Tremblay: Phys. Rev. Lett. **74** (1995) 968.

[44] We here ignore the misfit of the rungs in the neighboring ladders which exists in real $Sr_{14-x}Ca_xCu_{24}O_{41}$ compounds, since we take the continuum limit along the leg and consequently the misfit never appears in the present theory.

[45] M.Troyer, H.Tsunetsugu, and D.Würtz: Phys. Rev.**B50**(1994)13515.

[46] In the case of the 2nd order RG, the strong coupling values, $+1$ and -1, are replaced with $+\infty$ and $-\infty$, respectively.

[47] K. Yamaji :J. Phys. Soc. Jpn. **59** (1990) 677.

[48] H. Suhl, B.T. Mattis and L. R. Walker : Phys. Rev. Lett. **3** (1959) 552.

[49] J. Kondo: Prog. Theoret. Phys **29** (1963) 1.

[50] H. Kontani and K. Ueda: unpublished.

[51] H. J. Schulz: Phys. Rev. Lett. **64** (1990) 2831.

[52] N. Kawakami and S. K. Yang: Phys. Lett. **148** (1990) 359.

[53] H. Frahm and V. E. Korepin: Phys. Rev.**B 42** (1990) 10553.

[54] P. W. Anderson: Phys. Rev. Lett. **67** (1991) 3844.

[55] C. Castellani, C. D. Castro and W. Metzner: Phys. Rev. Lett. **69** (1992) 1703.

[56] D. G. Clarke, S. P. Strong and P. W. Anderson: Phys. Rev. Lett. **72** (1994) 3218.

[57] A. M. Tsvelik: preprint

Fig. 1: Array of Hubbard ladders studied here.

Fig. 2: Schematic illustrations of the one-particle process and the two-particle process (in the d-wave superconductivity channel). In the one-particle process, a particle hops from one ladder to a neighboring one, while in the two-particle process, a pair of particles (bipolaron) hops from one ladder to a neighboring one.

Fig. 3: (a) Four branches(LB, LA, RA, RB) of linearized bands with the bandwidth cutoff E, and (b) intraladder two-particle scattering vertices $g_\mu^{(i)}$. The solid and broken lines represent the propagators for the right-moving and left-moving electrons, respectively. m and $\bar{m}$ denote different bands.

Fig. 4: Diagrams which contribute to the 3rd order vertex corrections, (a) to the intraladder backward scattering processes $g_\mu^{(1)}$, (b) to the intraladder forward scattering processes $g_\mu^{(2)}$, and (c) to the intraladder self-energy processes. Wavy lines represent one of the intraladder scattering vertices, $g_\mu^{(i)}$ ($i = 1,\ 2;\ \mu = 0,\ f,\ t$).

Fig. 5: Diagrammatic representation of the scaling equation for the interladder one-particle hopping amplitude. A zigzag line represents the interladder one-particle hopping, $t_\perp$.

Fig. 6: Scaling flows of the interladder one-particle hopping amplitude, $t_\perp$, (a) for $\tilde{U} = 0.3$, and (b) for $\tilde{t}_{\perp 0} = 0.01$. For smaller $\tilde{U}$ and larger $\tilde{t}_{\perp 0}$, $\tilde{t}_\perp(l)$ exceeds unity in the course of the scaling.

Fig. 7: Diagrammatic representations of the generators of the interladder two-particle hopping processes, f_μ^M, (a) for the density wave channels, and (b) for the superconducting channels. The first, second and third lines correspond to the flavor indices $\mu = 0, f$ and t, respectively. Hatched circles represent the coupling strengths, g_μ^M.

Fig. 8: Diagrammatic representations of the leading order scaling equations for the two-particle hopping amplitudes, V_μ^M, (a) for the density wave channels (M =CDW or SDW), and (b) for the superconducting channels (M =SS or TS). Hatched squares represent V_μ^M.

Fig. 9: (a), (b), (c) Scaling flows of the intraladder coupling strengths for the composite fields, g_μ^M, and (d), (e), (f) scaling flows of the interladder two-particle hopping amplitudes, V_μ^M, for $\tilde{U} = 0.2,\ 0.3,\ 0.4$, respectively, and $\tilde{t}_{\perp 0} = 0.01$. The vertical broken line corresponds to the scaling parameter, l_c, at which $V^{\mathrm{SC}d}$ diverges.

Fig. 10: Scaling flows of the stiffness of the total-spin mode, $K_{\sigma+}$, the interladder one-particle hopping amplitude, $\tilde{t}_\perp$, and the interladder two-particle hopping amplitude in the SCd channel, V^{SCd}, for various initial conditions $(\tilde{U}, \tilde{t}_{\perp 0})$. For the region, $l > \mathrm{Min}(l_{\mathrm{c}}, l_{\mathrm{cross}})$, the scaling flows, drawn by broken curves, have no physical meaning, since the weak coupling picture breaks down in the region.

Fig. 11: Phase diagram of the weakly coupled Hubbard ladder system spanned by $\tilde{t}_{\perp 0}$ and the reduced temperature $\tilde{T} = T/E_0$ for $\tilde{U} = 0.3$. **SGM**, **SCd** and **2D** denote the sping gap metal phase, the d-wave superconducting phase and the two-dimensional phase, respectively. Gradual chanage of darkness in the SGM phase schematically depicts the gradual approach of the isolated systems to their low-energy asymptotics. Thick broken lines denote the crossover boundaries.

Fig. 12: Phase diagram of the weakly coupled Hubbard ladder system spanned by the intraladder Hubbard repulsion $\tilde{U}$ and the reduced temperature $\tilde{T} = T/E_0$ for $\tilde{t}_{\perp 0} = 0.01$. Gradual chanage of darkness in the SGM phase schematically depicts the gradual approach of the isolated systems to their low-energy asymptotics.Thick broken lines denote the crossover boundaries.

Fig. 13: Dependence of the crossover value of the interladder one-particle hopping amplitude, $\tilde{t}_{\perp c}$, on the intraladder Hubbard repulsion, $\tilde{U}$. For $\tilde{t}_{\perp 0} > \tilde{t}_{\perp c}$, the system undergoes the crossover to the 2D phase, while for $\tilde{t}_{\perp 0} < \tilde{t}_{\perp c}$, the SGM phase transits to the SCd phase.

Fig. 14: (a) Coupled ladder system with the misfit of the rungs in the neighboring ladders which actually exists in real $Sr_{14-x}Ca_xCu_{24}O_{41}$ compounds and (b) static interband polarization, $\chi_{AB}(q_\parallel, q_\perp)$, on the 1st Brillouin zone along the line $\Gamma(0,0) \rightarrow \mathrm{X}(\pi,0) \rightarrow \mathrm{M}(\pi,\pi) \rightarrow \Gamma$ for $t''/t = 0, 0.2, 0.3$ and temperature, $T = 10^{-5}t$.

Fig. 15: (a) Two branches(L, R) of linearized bands with the bandwidth cutoff E, and (b) intrachain two-particle scattering vertices $g^{(i)}$. The solid and broken lines represent the propagators for the right-moving and left-moving electrons, respectively.

Fig. 16: Scaling flows of the interchain one-particle hopping amplitude, $\tilde{t}_{\mathrm{chain}\perp}$ (the upper half plane), and the interchain two-particle hopping amplitude in the SDW channel, V^{SDW} (the lower half plane), for $\tilde{U} = 0.1$, 0.2, 0.3, and $\tilde{t}_{\perp 0} = 0.01$.

Fig. 17: Phase diagrams of the weakly coupled chains, (a) for $\tilde{U} = 0.3$, and (b) for $\tilde{t}_{\mathrm{chain}\perp 0} = 0.01$. **TL** and **2D** denote the Tomonaga-Luttinger liquid phase and the two-dimensional phase, respectively. Thick broken lines denote the crossover boundaries.

Fig. 18: Division of the four branches of the linearized bands into the inner region, $C_{\nu m<}$, and the outer shell, $d\mathcal{C}_{\nu m>}$.

Fig. 19: All labeled diagrams which renormalize $\mathcal{G}_{RB}(K_\parallel)$. Possible combinations of the band indices are $m_1m_2m_3 = BBB, ABA, BBA$. Inserted arrows with the labels I and II denote the outer-shell modess in the cases I and II, respectively.

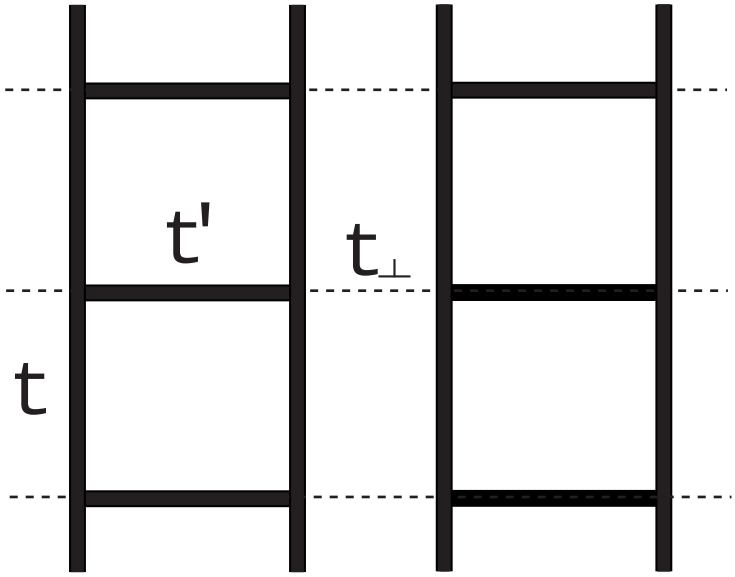

Fig.1

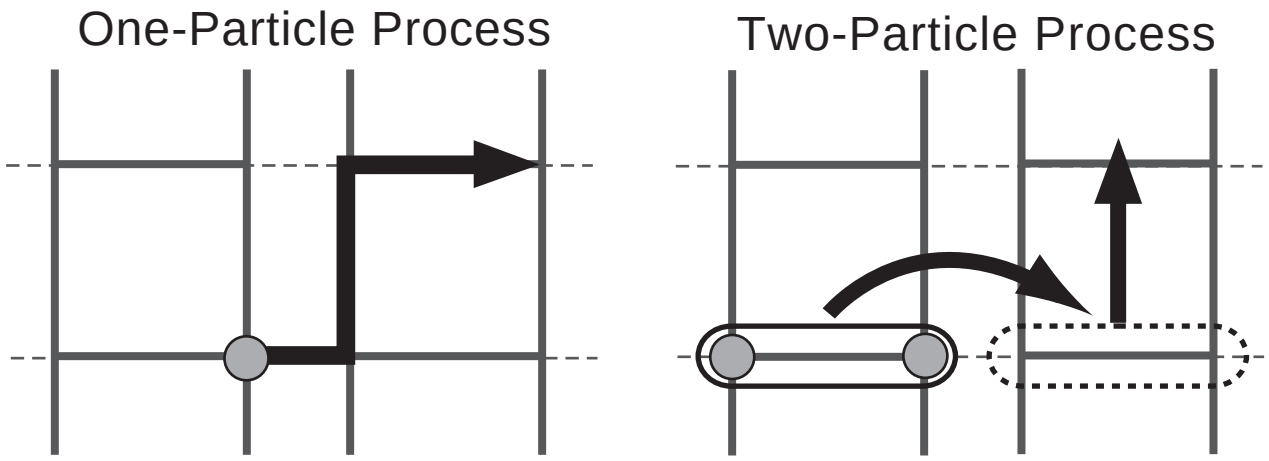

Fig.2

(a)

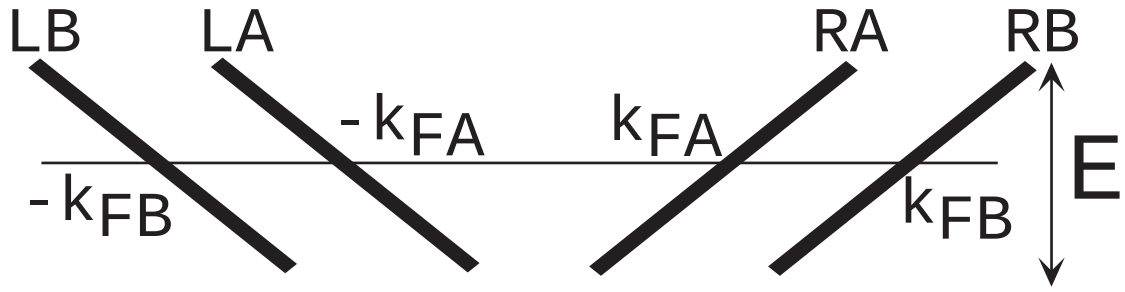

(b)

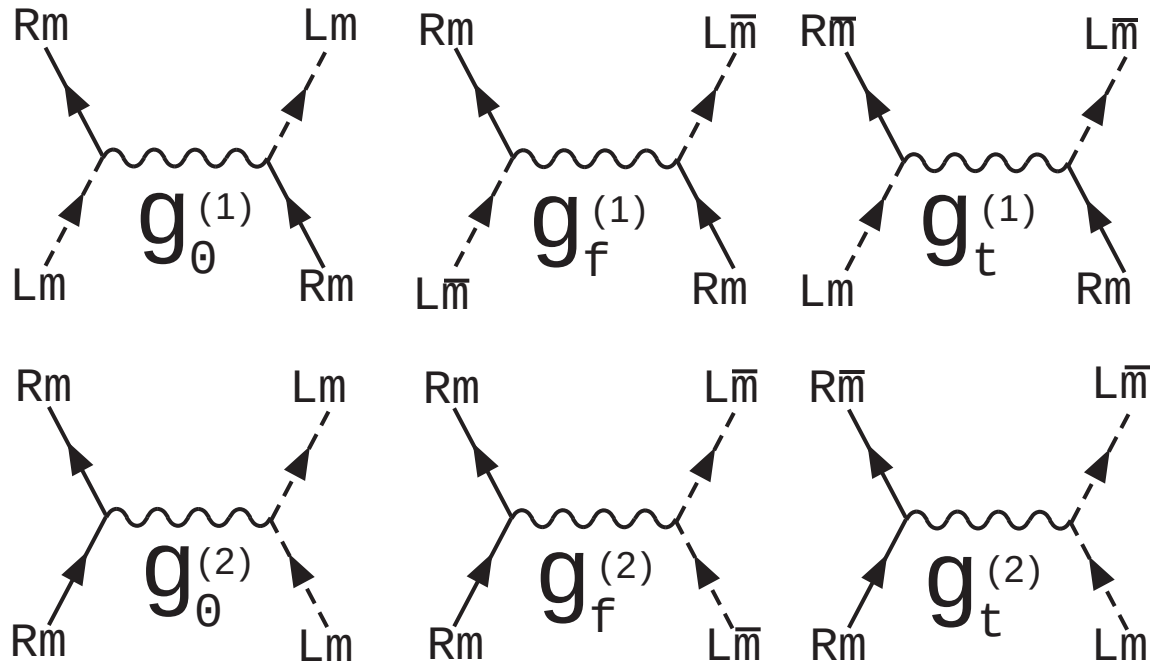

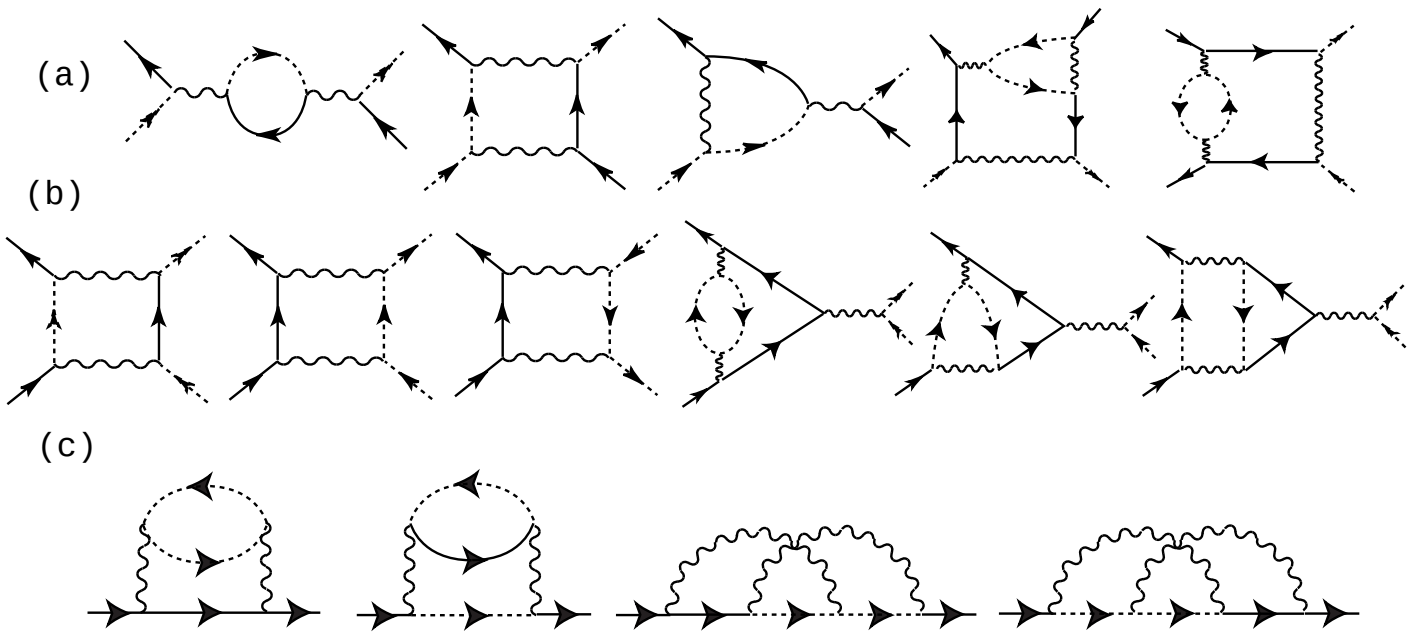

Fig.4

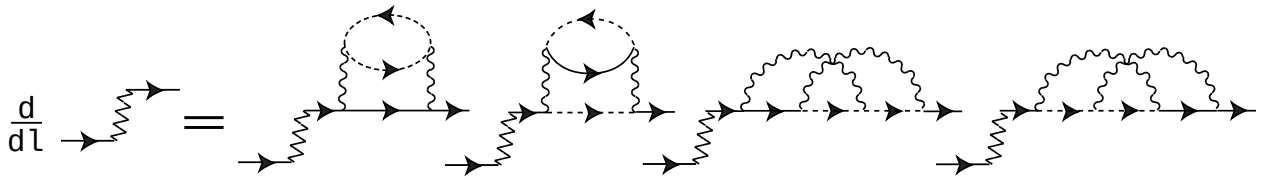

Fig.5

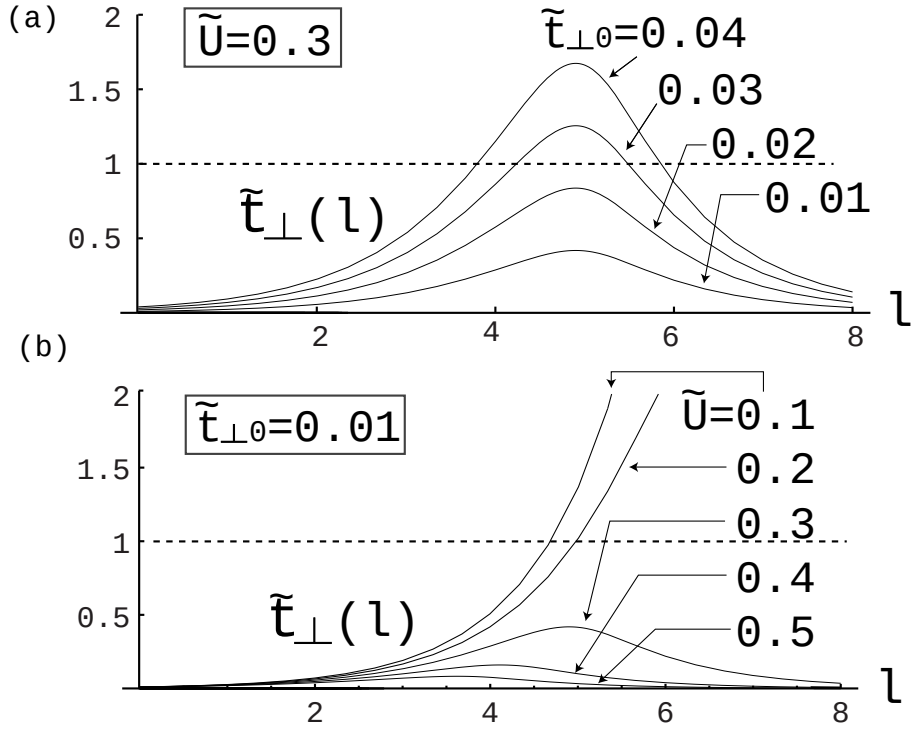

Fig.6

(a) CDW or SDW

0-process

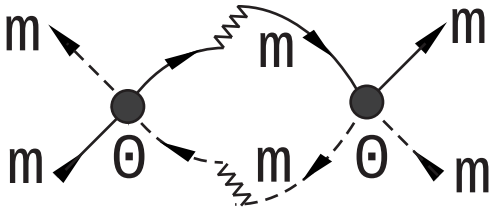

f-process

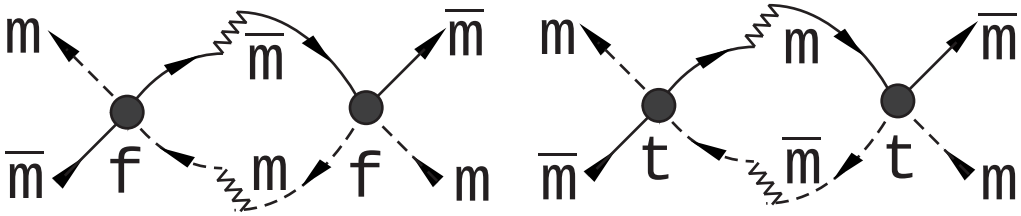

t-process

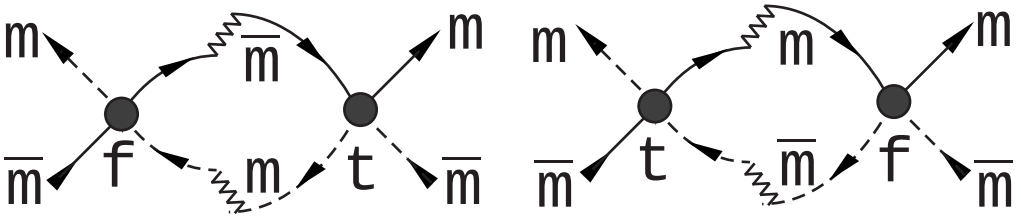

(b) SS or TS

0-process

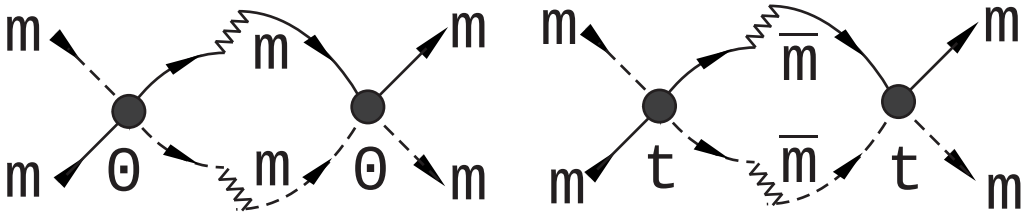

f-process

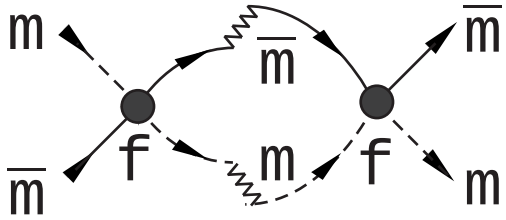

t-process

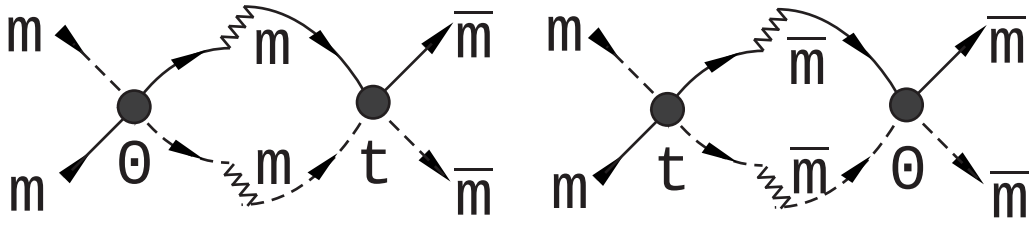

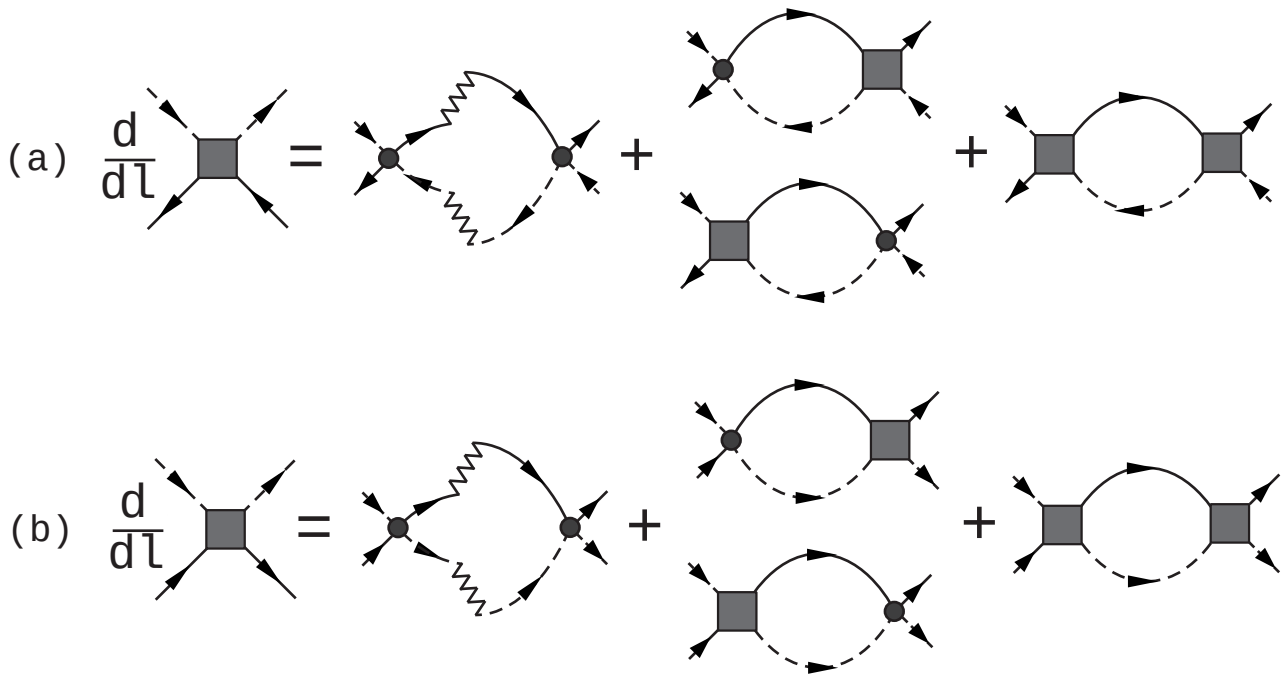
(a)
d/dl
=
+
+
(b)
d/dl
=
+
+

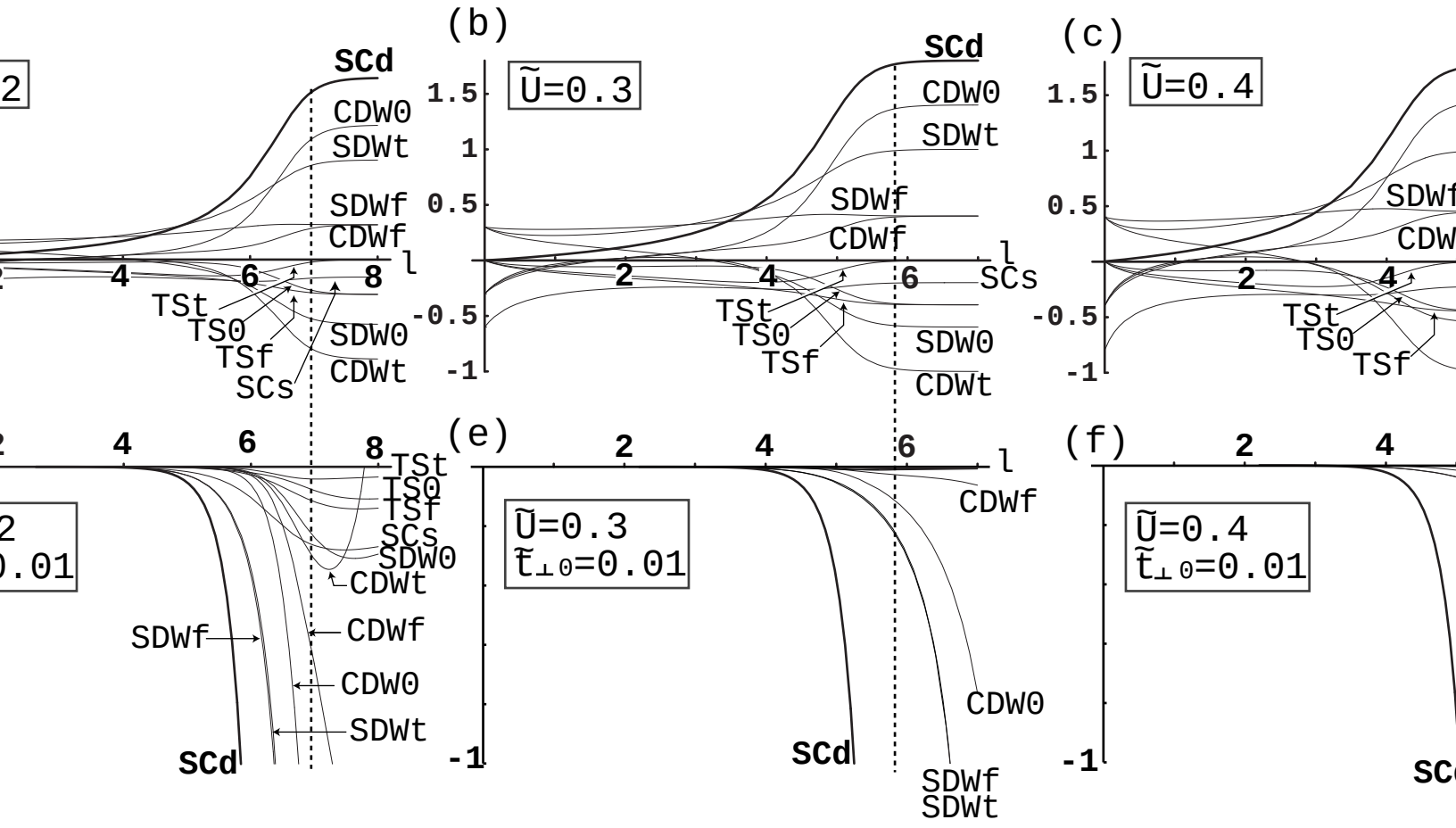
(b)
(c)
(e)
(f)
SCd
CDW0
SDWt
SDWf
CDWf
SDW0
CDWt
TSt
TS0
TSf
SCs
l
1.5
1
0.5
-0.5
-1
2
4
6
8
$\tilde{U}$=0.3
$\tilde{U}$=0.4
$\tilde{t}_{\perp 0}$=0.01

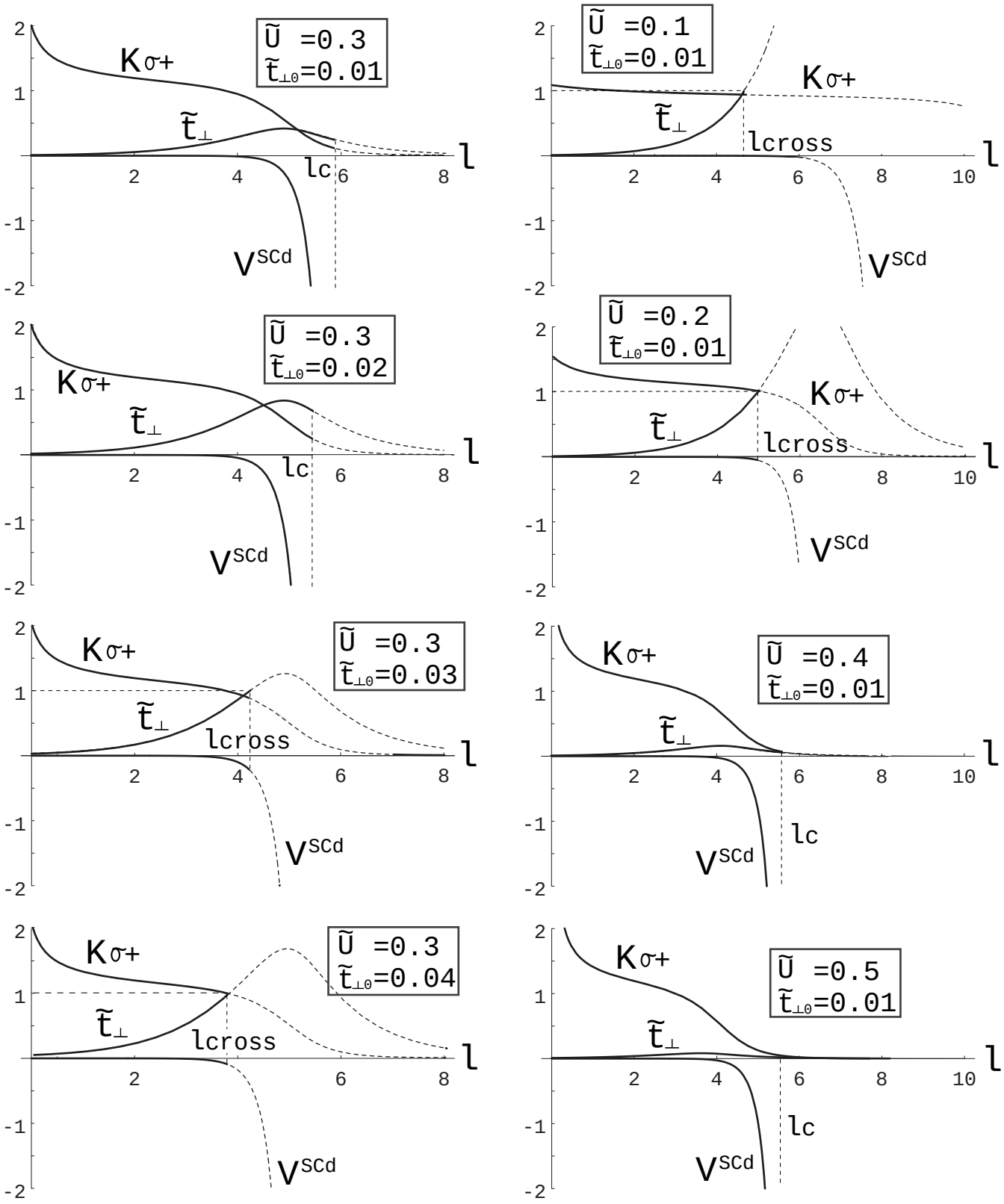
Ũ =0.3
t̃⊥0=0.01
Kσ+
t̃⊥
lc
l
VSCd
Ũ =0.1
t̃⊥0=0.01
Kσ+
t̃⊥
lcross
l
VSCd
Ũ =0.3
t̃⊥0=0.02
Kσ+
t̃⊥
lc
l
VSCd
Ũ =0.2
t̃⊥0=0.01
Kσ+
t̃⊥
lcross
l
VSCd
Ũ =0.3
t̃⊥0=0.03
Kσ+
t̃⊥
lcross
l
VSCd
Ũ =0.4
t̃⊥0=0.01
Kσ+
t̃⊥
lc
l
VSCd
Ũ =0.3
t̃⊥0=0.04
Kσ+
t̃⊥
lcross
l
VSCd
Ũ =0.5
t̃⊥0=0.01
Kσ+
t̃⊥
lc
l
VSCd

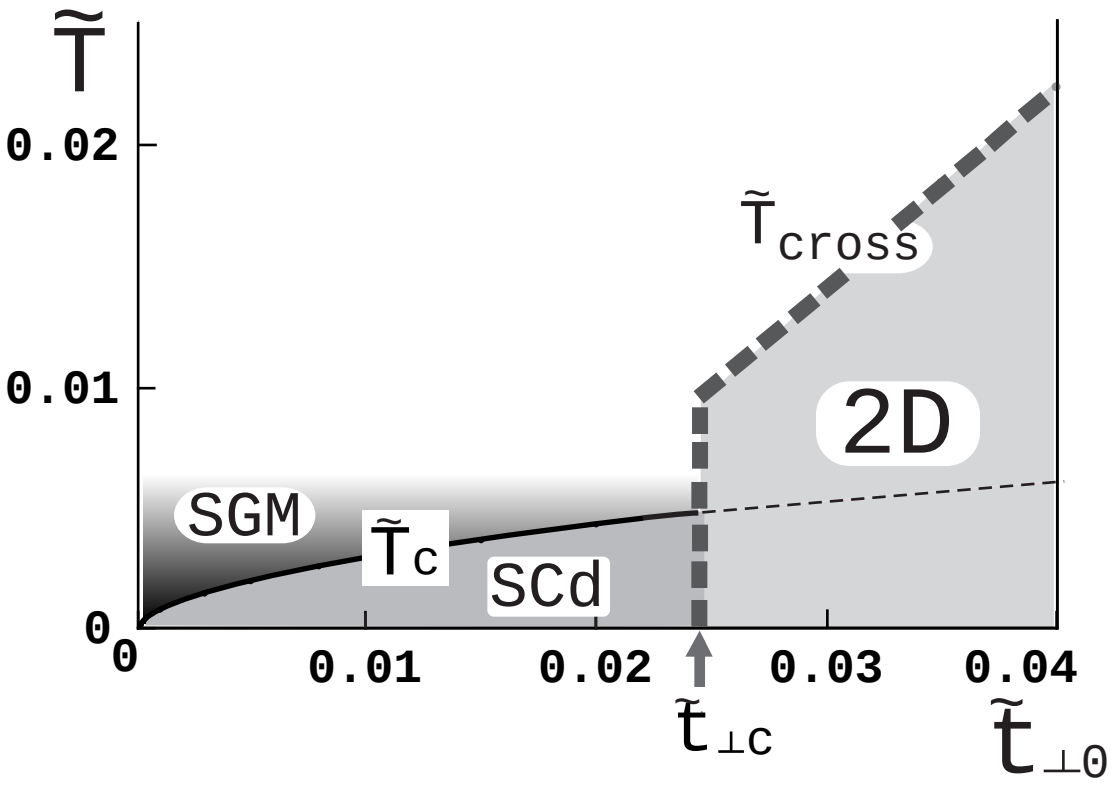
T̃
0.02
0.01
0
0
0.01
0.02
0.03
0.04
T̃cross
2D
SGM
T̃c
SCd
t̃⊥c
t̃⊥0

Fig.11

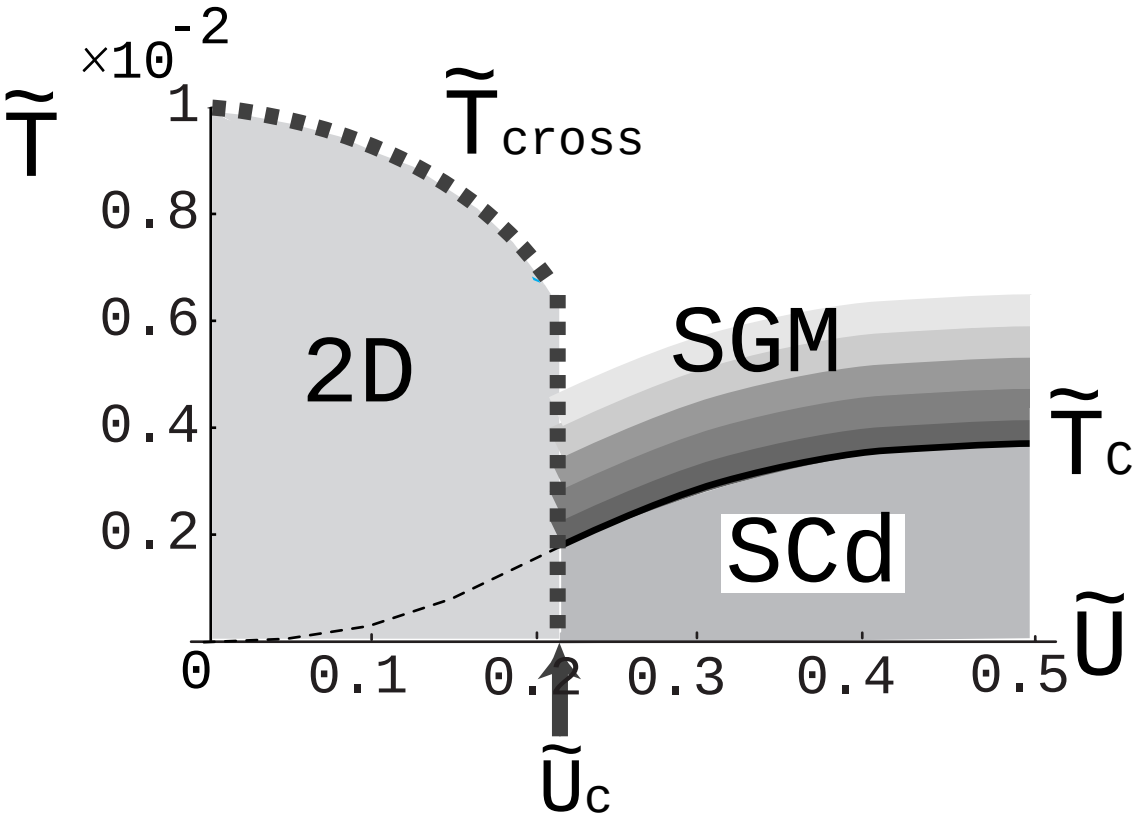
×10-2
T̃
1
0.8
0.6
0.4
0.2
0
T̃cross
2D
SGM
T̃c
SCd
0.1
0.2
0.3
0.4
0.5
Ũ
Ũc

Fig.12

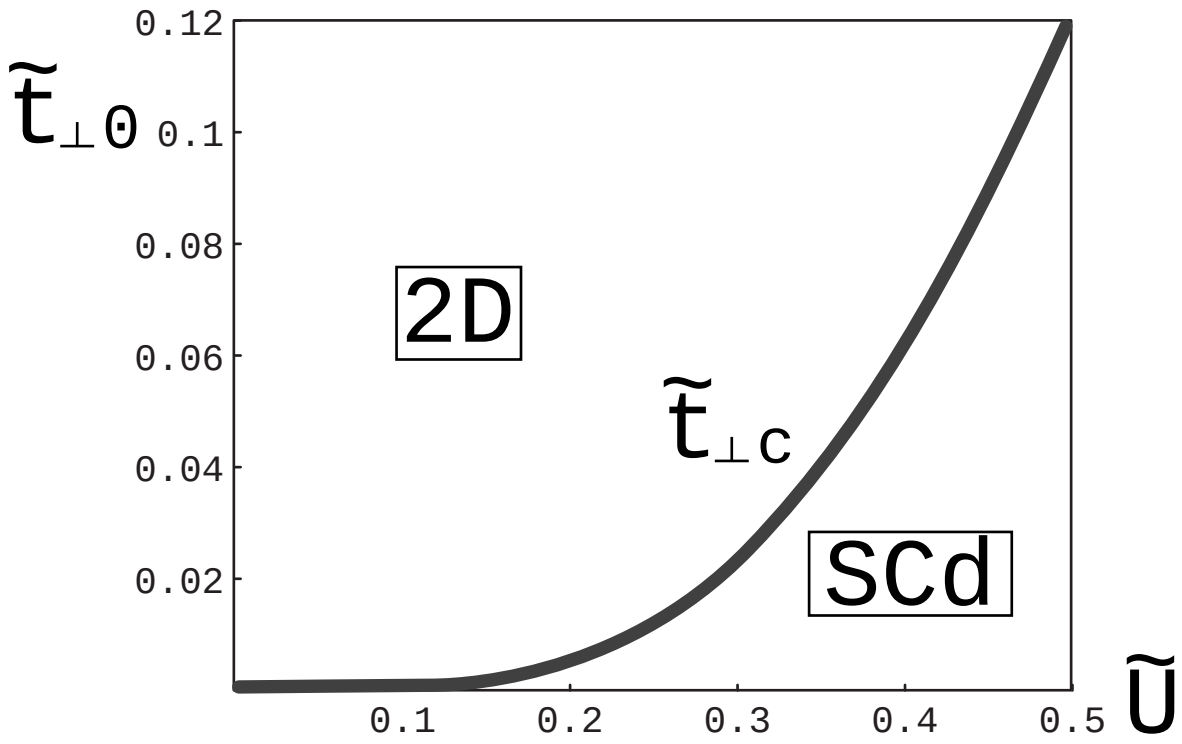
0.12
$\tilde{t}_{\perp 0}$ 0.1
0.08
0.06
0.04
0.02
2D
$\tilde{t}_{\perp c}$
SCd
0.1
0.2
0.3
0.4
0.5
$\tilde{U}$

(a)

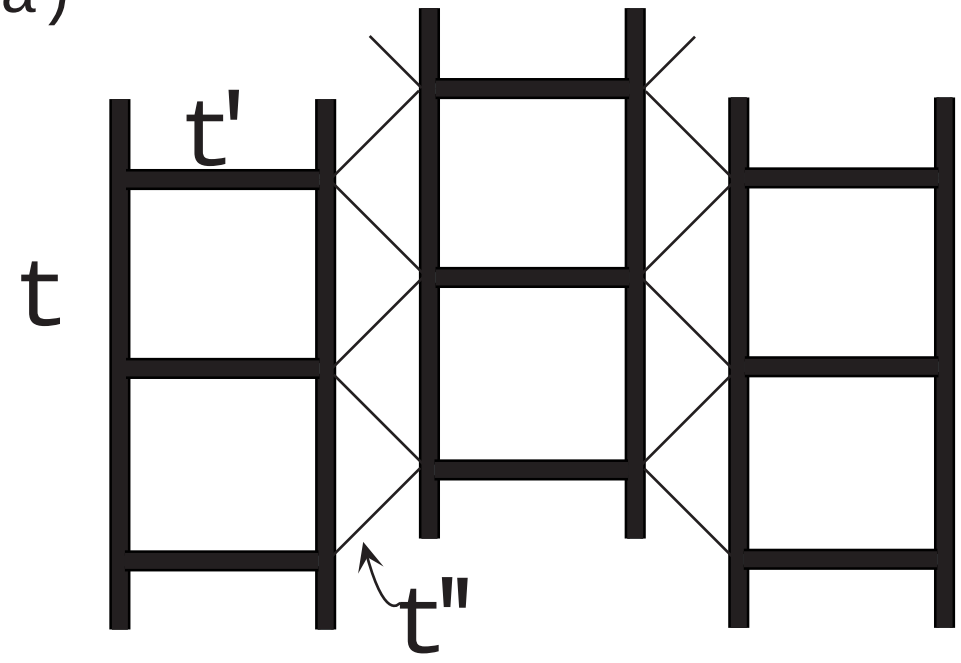

(b)

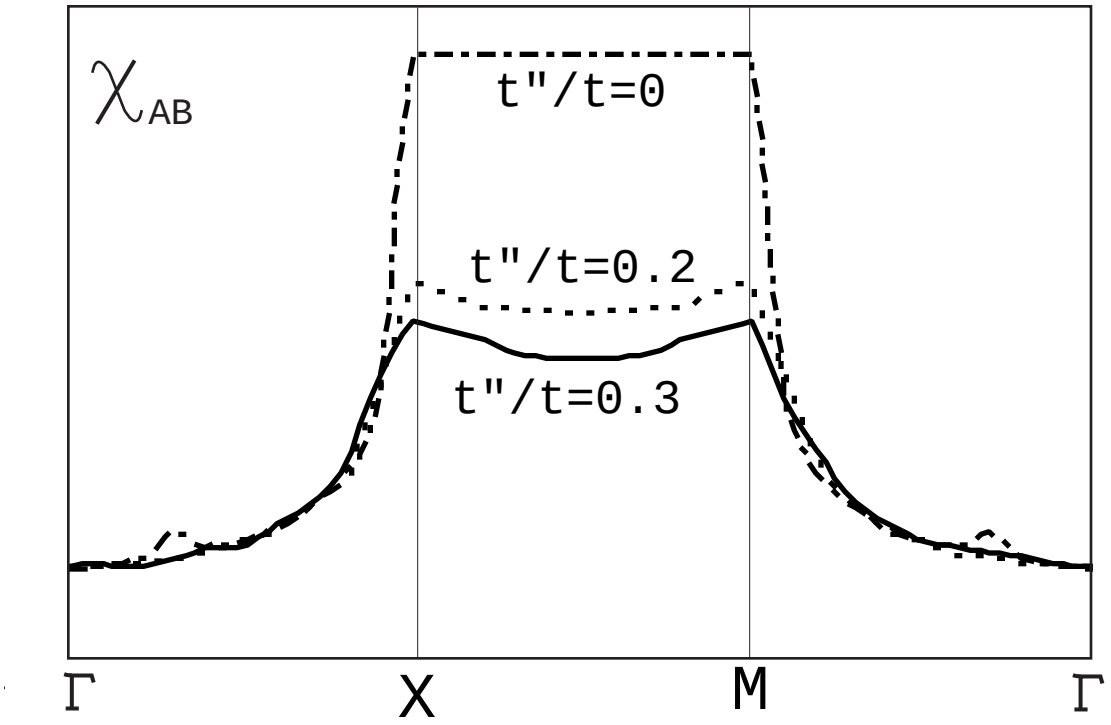

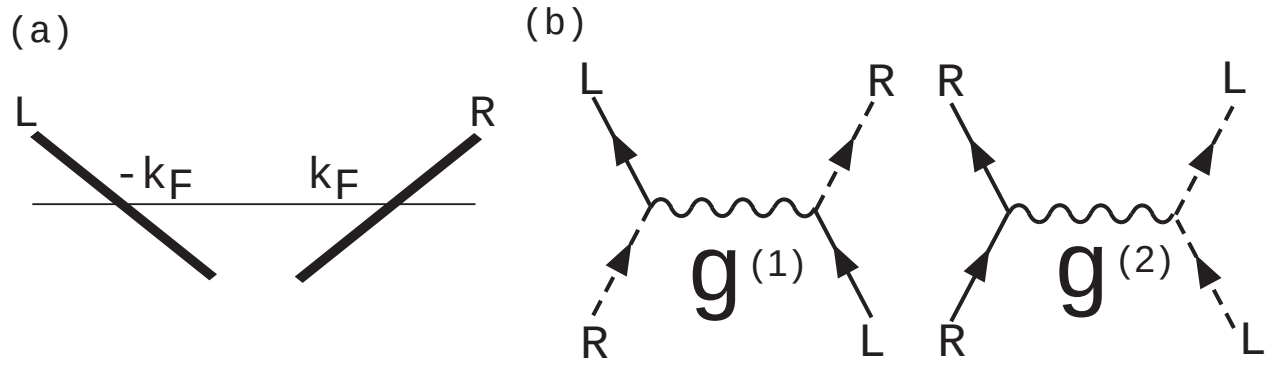
(a)
L
R
-k_F
k_F
(b)
L
R
R
L
g(1)
R
L
R
L
g(2)
R
L

Fig.15

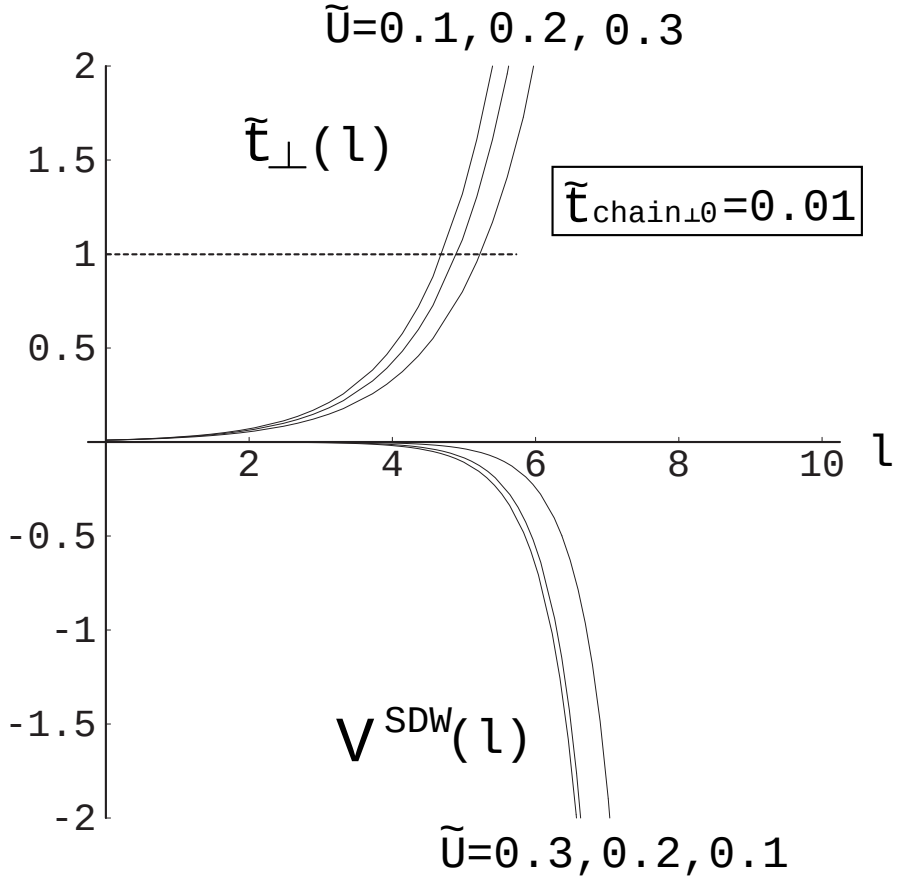
Ũ=0.1,0.2,0.3
t̃⊥(l)
t̃chain⊥0=0.01
V^SDW(l)
Ũ=0.3,0.2,0.1
l
2
1.5
1
0.5
-0.5
-1
-1.5
-2
2
4
6
8
10

Fig.16

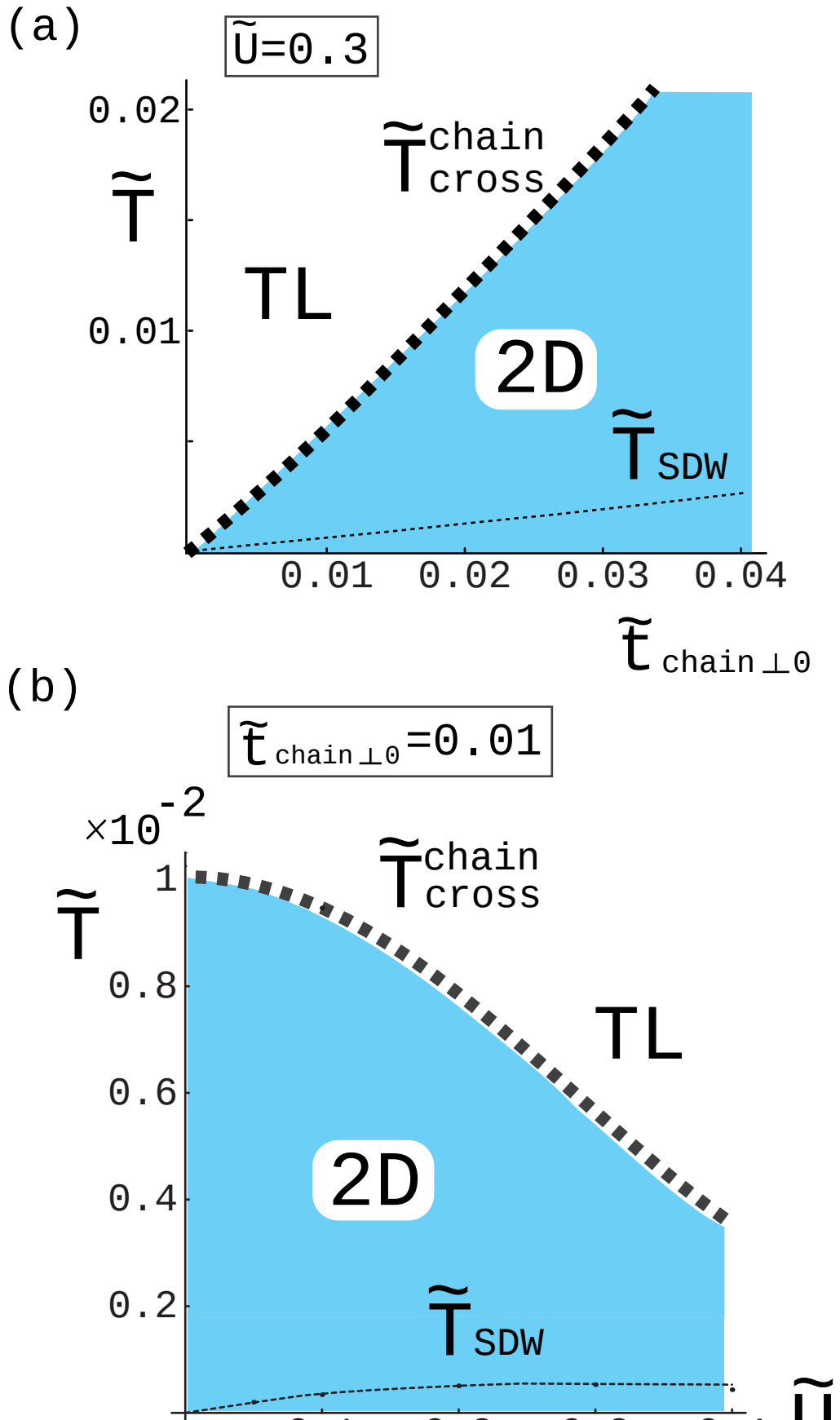
(a)
Ũ=0.3
0.02
0.01
T̃
T̃chain cross
TL
2D
T̃SDW
0.01
0.02
0.03
0.04
t̃chain⊥0
(b)
t̃chain⊥0=0.01
×10-2
1
0.8
0.6
0.4
0.2
T̃
T̃chain cross
TL
2D
T̃SDW
Ũ

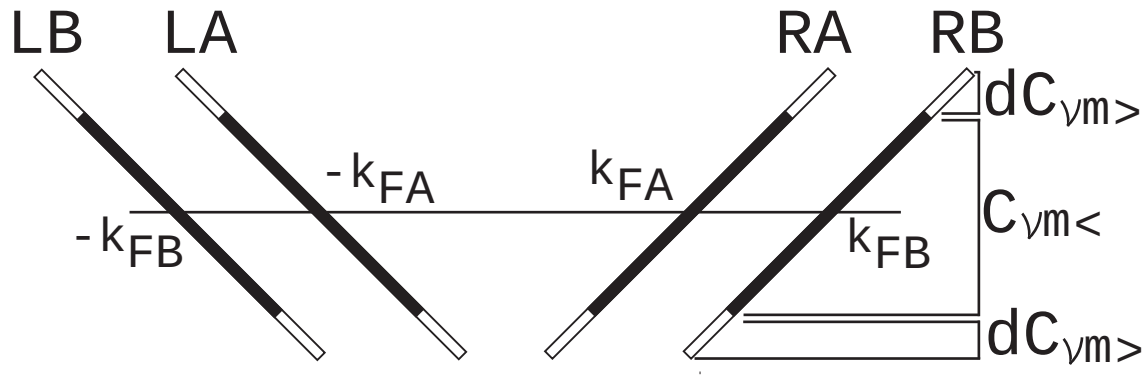
LB
LA
RA
RB
$dC_{\nu m>}$
$-k_{FA}$
k_{FA}
$-k_{FB}$
k_{FB}
$C_{\nu m<}$
$dC_{\nu m>}$

Fig.18

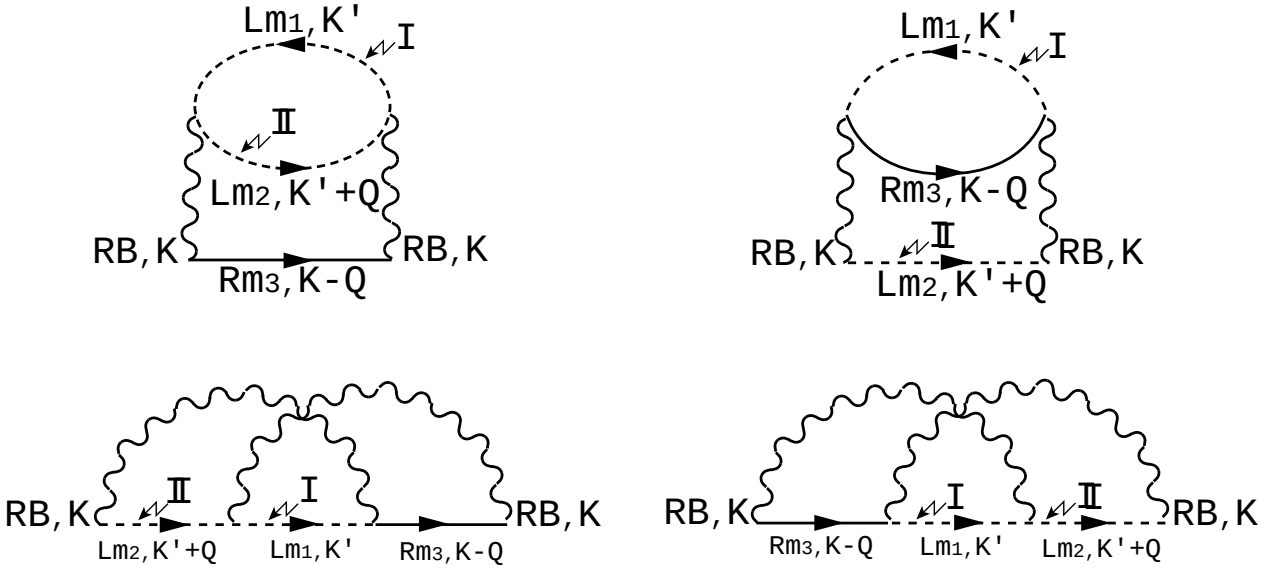
Lm1,K'
I
II
Lm2,K'+Q
RB,K
RB,K
Rm3,K-Q
Lm1,K'
I
Rm3,K-Q
RB,K
II
RB,K
Lm2,K'+Q
RB,K
II
I
RB,K
Lm2,K'+Q
Lm1,K'
Rm3,K-Q
RB,K
Rm3,K-Q
I
Lm1,K'
II
Lm2,K'+Q
RB,K

Fig.19